NEUROSCIENCE

Activity-regulated synaptic targeting of lncRNA ADEPTR mediates structural plasticity by localizing Sptn1 and AnkB in dendrites

Eddie Grinman[1], Yoshihisa Nakahata[2], Yosef Avchalumov[1], Isabel Espadas[1], Supriya Swarnkar[1], Ryohei Yasuda[2], Sathyanarayanan V. Puthanveettil[1]*

Activity-dependent structural plasticity at the synapse requires specific changes in the neuronal transcriptome. While much is known about the role of coding elements in this process, the role of the long noncoding transcriptome remains elusive. Here, we report the discovery of an intronic long noncoding RNA (lncRNA)—termed ADEPTR—that is up-regulated and synaptically transported in a cAMP/PKA-dependent manner in hippocampal neurons, independently of its protein-coding host gene. Loss of ADEPTR function suppresses activity-dependent changes in synaptic transmission and structural plasticity of dendritic spines. Mechanistically, dendritic localization of ADEPTR is mediated by molecular motor protein Kif2A. ADEPTR physically binds to actin-scaffolding regulators ankyrin (AnkB) and spectrin (Sptn1) via a conserved sequence and is required for their dendritic localization. Together, this study demonstrates how activity-dependent synaptic targeting of an lncRNA mediates structural plasticity at the synapse.

INTRODUCTION

Activity-dependent structural plasticity of neuronal synapses is a critical component of adaptive brain functions, such as long-term memory, and requires changes in the expression of transcriptional networks. The protein-coding factors of this transcriptional response to neuronal activation have been well studied and include proteins such as Arc (*1*), Camk2a (*2*), Homer1a (*3*), and BDNF (brain-derived neurotrophic factor) (*4*) that are distally transported and translated locally at activated synapses (*5*, *6*). These gene products then facilitate the structural reorganization therein by acting as signaling factors, scaffolds for the cytoskeleton, receptor subunits, and more (*7*).

Recent advances in next-generation sequencing studies have led to a deeper understanding of the components of the transcriptome, notably that it contains several thousands of large RNA products (*8*) that do not code for protein (*9*). While the vast majority of these long noncoding RNAs (lncRNAs) have yet to be experimentally interrogated and their role in mediating synapse function is poorly understood, lncRNAs have previously been profiled that contribute to neuronal function by regulating target mRNA or ribosomal RNA (rRNA) transcription and processing in the nucleus (*10*, *11*) or interacting with microRNAs (miRNAs) in the cytoplasm (*12*).

A major consequence of activity-dependent transcriptional changes is the transport of RNAs for remodeling of preexisting synapses and formation of new ones. Although the significance of mRNAs that are transported have previously been investigated (*13*, *14*) from the soma to the synapse for local translation and structural plasticity, it is unknown whether lncRNAs are transported to synapses for synaptic changes and the underlying mechanisms therein. Of intrigue, lncRNAs are known to display activity-dependent responses similar to mRNAs in neurons (*15*) but show higher turnover rates (*16*). Concurrently, we have little knowledge about whether and how lncRNAs can be distally transported during activity-dependent plasticity changes at the synapse.

Here, we report the discovery as well as the functional and mechanistic characterization of an activity-dependent lncRNA that is distally transported in mouse hippocampal neurons. We found that this lncRNA is rapidly expressed and transported to distal processes, is necessary for activity-dependent structural plasticity, and functionally interacts with the spectrin/ankyrin network in dendrites through a domain conserved in human 3′ untranslated regions (3′UTRs).

RESULTS

Discovery of an activity-dependent synaptically targeted lncRNA

We used a multipronged approach to begin uncovering lncRNAs that are robustly expressed and transported in activated hippocampal neurons, as summarized in Fig. 1A. We first profiled lncRNA expression in mature primary hippocampal neurons that were exposed to forskolin (FSK) to activate cAMP signaling, a signaling cascade known to mediate long-term potentiation in cultured neurons and learning in vivo (*17*–*19*). Total RNA isolated from three biological replicates per group were subjected to next-generation RNA sequencing (RNA-seq), clustering, and differential expression analysis (fig. S1, A and B). In addition to previously known immediate early genes (Fos, Egr2, Nr4a1, and Arc), using gene biotype analysis, we observed numerous Ensembl-annotated lncRNAs from varying genomic origins (fig. S1B). We then asked whether cAMP-regulated lncRNAs are enriched distally from the soma by using a fractionation strategy to generate hippocampal synaptoneurosomes (fig. S2, A and B). We validated the enrichment quality of the preparations by immunoblotting for pre- and postsynaptic markers synaptophysin and PSD-95 (post synaptic density protein 95) (fig. S2C). We then isolated the RNA therein (fig. S2D) and systematically screened lncRNA candidates by quantitative reverse transcription polymerase chain reaction (qRT-PCR) (fig. S2E and table S1).

[1]Department of Neuroscience, Scripps Research, 130 Scripps Way, Jupiter, FL 33458, USA. [2]Max Planck Florida Institute for Neuroscience, Jupiter, FL 33458, USA. *Corresponding author. Email: sputhanv@scripps.edu

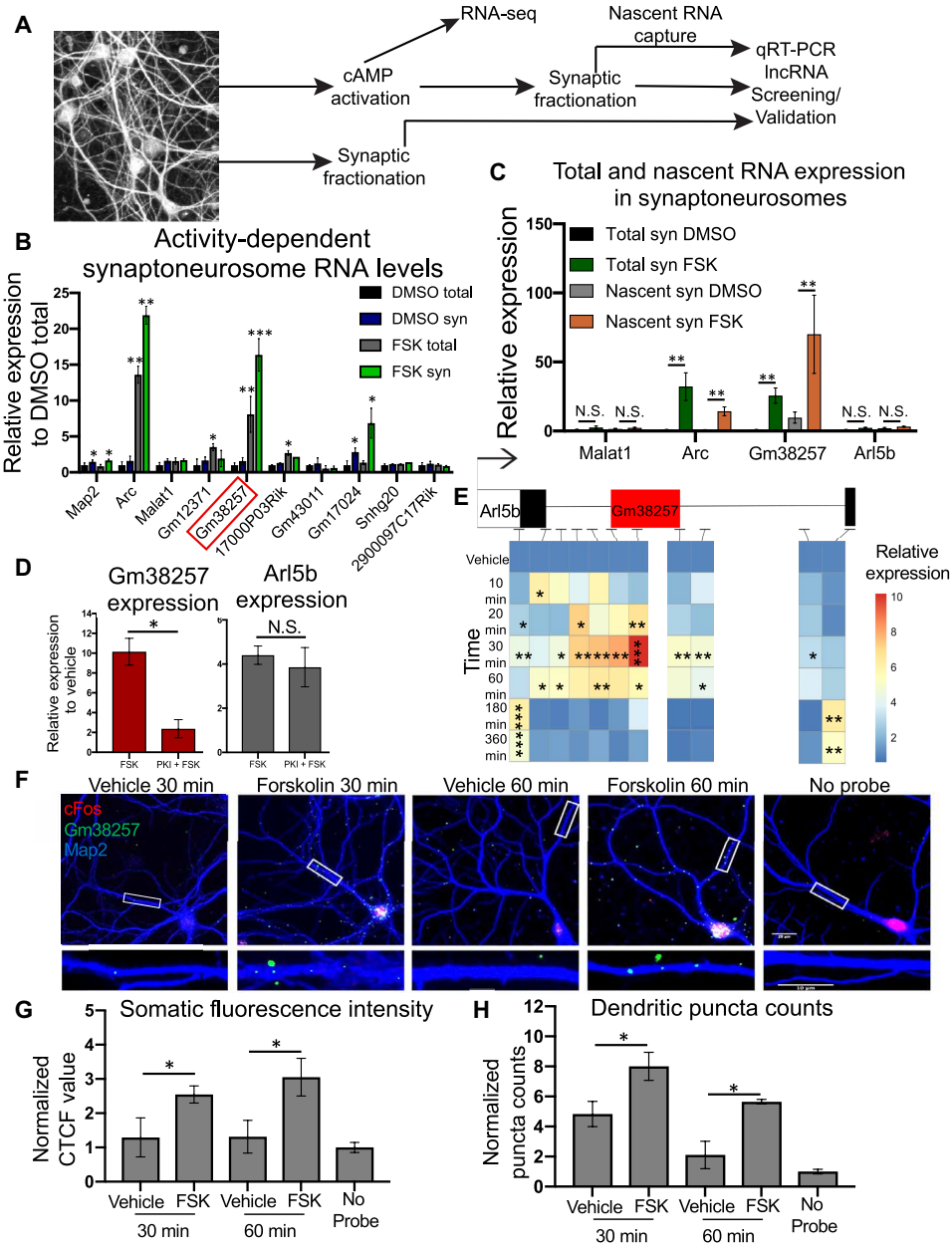

Fig. 1. Gm38257 is a novel lncRNA that is expressed in hippocampal neurons and dendritically localized in a cAMP-dependent manner. (**A**) Schematic of approach to identify activity-dependent synaptically targeted lncRNAs. (**B**) RNA was isolated from synaptoneurosome fractions or total lysates from FSK or vehicle-treated neurons. qRT-PCR was performed on $N = 3$ to 4 independent wells using 18*S* RNA as internal control. $^{*}P < 0.05$ and $^{**}P < 0.01$, Dunnett's test compared to vehicle total. (**C**) EU nucleotides were incorporated into nascent RNA followed by forskolin or vehicle treatment and synaptosome preparation. Total synaptic RNA was extracted before click chemistry–based nascent RNA capture. "Total" and "nascent" indicate total and nascent RNA from synaptoneurosomes. Malat1 and Arc were used as negative and positive controls, respectively. One-way ANOVA and Tukey's post hoc test, $N = 6$ to 7 wells per group from three experiments. N.S., not significant. (**D**) DIV 16 primary hippocampal neurons were treated with forskolin for 30 min or 14-22 amide protein kinase inhibitor (PKI) for 30 min and forskolin for another 30 min before RNA isolation and qRT-PCR. $^{*}P < 0.05$, unpaired, two-sided t test. $N = 3$ to 4 wells per group. (**E**) Heatmap showing expression of Arl5b exons and introns at the indicated time points, relative to vehicle. Asterisks represent statistical significance relative to vehicle by Dunnett's test. $N = 3$ to 5 wells per group, $^{***}P < 0.001$. (**F**) Neurons were fixed and processed for FISH using digoxygenin-labeled riboprobes. Cells were immunolabeled with Map2 to label dendrites and cFos to measure neuronal activation. (**G**) Somatic fluorescence intensity was measured using Corrected Total Cell Fluorescence measurement in ImageJ. (**H**) Extra somatic puncta were acquired by a custom ImageJ macros script; counts were normalized to no-probe control. $N = 17$ to 24 neurons per group from three experiments. $^{*}P < 0.05$ and $^{**}P < 0.01$, pairwise *t* test with Holm's correction. Error bars represent SEM. Scale bars, 20 μm (neuron image) and 10 μm (inset).

Analysis of synaptoneurosomes from neurons exposed to forskolin show that Gm38257 was the most robustly expressed and consistently enriched in a cAMP-dependent manner [fold change in Gm38257 expression in FSK synaptosomes compared to dimethyl sulfoxide (DMSO) total lysate: 16.38 ± 2.26, $P < 0.001$, DMSO synaptosomes compared to DMSO total lysate:1.55 ± 0.48, $P = 0.98$, one-way analysis of variance (ANOVA), Dunnett's test, $N = 3$ to 4 replicates per group] (Fig. 1B and table S1). We also studied the expression levels of Arc mRNA in synaptoneurosomes, a well-known activity-dependent synaptically targeted mRNA neurons (*20*), and found significant enrichment (fold change in Arc expression in FSK synaptosomes compared to DMSO total lysate: 21.88 ± 1.25, $P < 0.001$, DMSO synaptosomes compared to DMSO total lysate: 1.58 ± 0.66, $P < 0.14$, one-way ANOVA, Dunnett's test, $N = 3$ to 4 replicates per group) (Fig. 1B and table S1).

Intronic lncRNA Gm38257 is expressed in a cAMP-dependent manner uniquely from its host gene

Inspection of the genomic locus of Gm38257 revealed that it is a single-exon transcript located within the first intron of Arl5b, a protein-coding gene (fig. S3A). PhyloCSF (*21*) and Coding Potential Assessment Tool (*22*) both showed that Gm38257 is not likely to code for protein (fig. S3, A and B). qRT-PCR analysis from nuclear and cytoplasmic fractions revealed that both Gm38257 and Arl5b are up-regulated by cAMP signaling and are expressed in both nuclear and cytoplasmic fractions (fig. S4A). We next asked whether newly synthesized Gm38257 is distally targeted by nascent RNA capture analysis. Our measurements of total and nascent RNA captured from synaptoneurosomes show that Gm38257, but not Arl5b, is enriched in synaptoneurosomes upon forskolin stimulation (table S1; Gm38257 nascent RNA with FSK versus nascent RNA with DMSO: $P = 0.02$, one-way ANOVA followed by Tukey's post hoc test; Arl5b: $P = 0.08$, one-way ANOVA, $N = 6$ to 7 per group) (Fig. 1C and table S1).

By performing a time course of cAMP signaling in hippocampal neurons and designing qPCR primers tiling the exons 1 and 2 and intron 1 of Arl5b, we found that Gm38257 and Arl5b have alternate expression patterns (Fig. 1D and table S1). We further determined that cAMP-dependent Gm38257 expression, but not Arl5b expression, is reduced by inhibition of cAMP-dependent protein kinase (PKA) with 14-22 amide, a cell-permeable protein kinase A inhibitor (PKI) (Gm38257 FSK + PKI versus Gm38257 FSK: $P = 0.012$, Arl5b FSK + PKI versus Arl5b FSK: $P = 0.72$, two-tailed unpaired t test, $N = 3$ to 4 per group) (Fig. 1E and table S1), suggesting that only Gm38257 expression is regulated by cAMP/PKA signaling. We then performed a comprehensive pharmacology screen in hippocampal neurons and found that Gm38257, but not Arl5b, was up-regulated by D1 receptor stimulation, KCl, and glutamate stimulation, as well as to forskolin treatment after tetrodotoxin (TTX) treatment (fig. S4B and table S1). We next asked whether the expression of Gm38257 might be regulated by activation of synaptic inhibitory signaling. Therefore, we analyzed the expression of Gm38257 in hippocampal neurons following exposure to γ-aminobutyric acid (GABA). Gm38257 was down-regulated by GABA stimulation, suggesting that its basal expression level is negatively regulated by inhibitory signaling (GABA versus vehicle, $P = 0.028$, Student's t test, $N = 4$ per group; fig. S4C and table S1). In these experiments, Arc mRNA was used as a positive control for immediate early gene expression (*23*) and appeared to be expressed similarly to Gm38257 (GABA versus vehicle, $P = 0.001$, Student's t test, $N = 4$ per group) (fig. S4, B and C). Together, these results suggest that Gm38257 is regulated by activity in a similar manner as Arc and independently of Arl5b.

Gm38257 is synaptically targeted in a cAMP-dependent manner, independently of its host gene

To confirm cAMP-dependent dendritic transport and localization of Gm38257 in hippocampal neurons, we performed RNA fluorescence in situ hybridization (FISH) in stimulated and unstimulated conditions. By costaining with Map2 to label dendrites and cFos to differentiate stimulated and unstimulated neurons, we confirmed that this lncRNA is globally up-regulated and dendritically localized at 30 and 60 min after stimulation (somatic RNA: FSK 30 min versus DMSO 30 min: $P = 0.04$, FSK 60 min versus DMSO 60 min: $P = 0.03$, dendritic RNA: FSK 30 min versus DMSO 30 min: $P = 0.02$, and FSK 60 min versus DMSO 60 min: $P = 0.01$, pairwise two-tailed t test with Holm correction, $N = 17$ to 24 neurons from three experiments) (Fig. 1, F to H, and table S1). We further observed that Gm38257 RNA puncta are distally localized in dendrites in a forskolin-dependent manner (fig. S5A). By quantifying the RNA puncta sizes into discrete bins (fig. S5, B and C, and table S1), we learned that the increase in dendritic expression of Gm38257 was specific to large-sized puncta (>0.5 μm²), indicating a reliable signal difference between stimulated and unstimulated conditions. Furthermore, we fit a linear regression model to determine the relationship between nuclear cFos expression with somatic and dendritic Gm38257 expression. cFos had a statistically significant positive relationship with both of these variables, indicating that cFos is a reliable predictor of Gm38257 expression (fig. S5D). Quantification of puncta every 5 μm from the middle of the soma showed that there was a statistically significant increase of puncta in forskolin-treated samples at distal positions (80 to 85 and 105 to 115 μm from the middle of the soma) compared to vehicle (fig. S5E and table S1). Consistent with our previous findings, Arl5b mRNA did not display activity-dependent dendritic localization (fig. S6, A to C). Malat1, an abundant nuclear enriched lncRNA, also showed no dendritic localization, as did the no probe control (fig. S6D).

To confirm whether Gm38257 levels are transcriptionally regulated, we treated neurons with the transcription initiation complex inhibitor, actinomycin D, before forskolin treatment. FISH analysis shows that activity-dependent somatic and dendritic localization of Gm38257 is significantly reduced. (fig. S7 and table S1) in the presence of actinomycin D, suggesting that cAMP signaling induced transcriptional changes in Gm38257. These results are consistent with our previous data showing that Gm38257 is enriched in synaptoneurosomes as a nascent RNA (Fig. 1C). Conversely, blocking ribosome function with anisomycin before forskolin stimulation did not result in decreased somatic or dendritic expression of Gm38257 (fig. S7 and table S S1). These results suggest that Gm38257 expression is dependent on transcriptional rather than post transcriptional processes.

RNA cargos that are synaptically targeted are known to require active transport along the microtubule and actin cytoskeleton (*24*). To confirm whether Gm38257 is likewise transported by cytoskeletal machinery, we blocked microtubule or actin cytoskeleton using inhibitors of polymerization nocodazole or cytochalasin D, respectively, before forskolin treatment. We found that both of these manipulations reduced the dendritic, but not the somatic, expression of Gm38257, suggesting that this lncRNA is actively transported to

dendrites and that integrity of the microtubule and actin cytoskeleton is required for its localization (fig. S8 and table S1). This is consistent with previous findings regarding the transport of the small ncRNA BC1 (*25*). Last, by labeling dendritic spines with green fluorescent protein (GFP) and costaining with actin, the primary cytoskeletal component of dendritic spines, we observed overlap of Gm38257 puncta with these spine markers, indicating that this lncRNA is localized to synaptic compartments (fig. S9). Given that Gm38257 is acutely regulated by neuronal activity and is distally transported as a nascent RNA upon expression, we have termed this transcript ADEPTR—activity-dependent transported lncRNA. Our results suggest that ADEPTR is an activity-dependent intronic lncRNA that is expressed and distally transported to synapses independent of its host mRNA.

lncRNA ADEPTR is required for activity-dependent changes in synaptic transmission and structural plasticity

We next investigated whether cAMP-dependent changes in ADEPTR expression levels play a role in hippocampal neuron function by using a loss-of-function analysis using antisense locked nucleic acid Gapmers, a strategy that has previously been used to ascertain lncRNA function in neurons (*11*). We transfected two independent Gapmers targeting ADEPTR, scrambled or no Gapmer for 48 hours into primary hippocampal neurons, and then extracted RNA after treating neurons with forskolin or DMSO (Fig. 2A). Both Gapmers significantly blunted the cAMP-dependent increase of ADEPTR in hippocampal neurons (untransfected + FSK: 7.5 ± 0.91, scrambled Gapmer + FSK: 6.8 ± 0.73, Gapmer1 + FSK: 3.7 ± 0.67, and Gapmer2 + FSK: 1.5 ± 0.47, $N = 4$ to 6 per group, $P < 0.05$, one-way ANOVA and Tukey's post hoc test) (Fig. 2B, fig. S10, and table S2). Gapmer2 was also effective in suppressing ADEPTR levels in basal conditions (untransfected + DMSO: 1.0 ± 0.09, scrambled Gapmer + DMSO: 0.98 ± 0.13, and Gapmer2 + DMSO: 0.24 ± 0.05, $P < 0.05$, one-way ANOVA and Tukey's post hoc test) (Fig. 2B and table S S2). Activity-dependent expression of Arc mRNA was not affected by either Gapmer (fig. S11A and table S S2), suggesting no difference in cAMP-induced immediate early gene expression changes between samples. Although Arl5b mRNA was also down-regulated by both Gapmers (fig. S11B), Western blotting showed that at 30 min after stimulation, Arl5b protein levels were neither affected by ADEPTR Gapmers nor by forskolin stimulation (fig. S11, C and D, and table S2). We therefore conclude that the Gapmers are efficient in lowering cAMP-dependent ADEPTR expression without affecting Arl5b.

A previous work has shown that cAMP signaling results in robust changes in synaptic transmission, as well as structural plasticity, in hippocampal neurons (*26*). We asked whether ADEPTR knockdown could influence neuron function in basal or cAMP-dependent conditions. We therefore performed live imaging of GFP-labeled hippocampal neurons in stimulated and unstimulated conditions and asked whether ADEPTR knockdown alters neuronal structural properties. By performing spine analysis, we found that both ADEPTR-targeting Gapmers suppressed cAMP-dependent changes in spine density (FSK + GFP: 50.59 ± 2.3, FSK + scrambled Gapmer: 47.87 ± 3.12, FSK + Gapmer1: 33.95 ± 3.32, FSK + Gapmer2: 26.8 ± 2.45, and DMSO + GFP: 29.38 ± 3.52, $P < 0.01$, one-way ANOVA and Tukey's post hoc test, $N = 16$ to 22 neurons from three experiments) (Fig. 2, C and D, and table S2). Specifically, the deficiency in spine number was specific to mushroom spines (FSK + GFP: 25.22 ± 2.5, FSK + scrambled Gapmer: 26.68 ± 3.19, FSK + Gapmer1: 13.24 ± 2.84, FSK + Gapmer2: 11.62 ± 1.82, and DMSO + GFP: 8.15 ± 1.67, $P < 0.01$, one-way ANOVA and Tukey's post hoc test) (Fig. 2E and table S2). Conversely, by performing Sholl analysis on these same neurons, we ascertained that neither ADEPTR knockdown nor cAMP signaling had an effect on neuronal branching (fig. S12 and table S2). We then measured the effect of ADEPTR knockdown on activity-dependent spontaneous excitatory postsynaptic currents (sEPSCs) using whole-cell patch-clamp recordings before and after forskolin stimulation (Fig. 2F). Knockdown of ADEPTR by two independent Gapmers suppressed the cAMP-dependent up-regulation of EPSC amplitude (untransfected: 60.16% ± 11.65, scrambled Gapmer: 55.91% ± 6.95, Gapmer1: 4.12% ± 7.41, and Gapmer2: 5.38 ± 5.78, $N = 22$ to 28 neurons from three experiments) but not frequency ($P = 0.6$, one-way ANOVA) (Fig. 2G and table S2). ADEPTR knockdown had no effect on basal EPSC amplitude or frequency suggesting that its role is specific to cAMP-dependent changes in synaptic transmission (Fig. 2H and table S2).

To confirm our findings by an alternate loss-of-function strategy, we cloned a short hairpin RNA (shRNA) cassette corresponding to the same sequence as Gapmer2 into a PLL3.7 shRNA plasmid with a lentiviral packaging backbone and GFP reporter. To confirm knockdown efficiency of this plasmid in neurons relative to scrambled shRNA plasmid, we packaged both into separate lentiviruses, transduced neurons, and collected RNA from FSK-treated or untreated conditions. Like the Gapmer2, the ADEPTR shRNA significantly suppressed ADEPTR expression in basal and forskolin conditions relative to the negative control (shADEPTR versus shNC: $P = 0.028$, shADEPTR + FSK versus shNC + FSK: $P = 0.017$, unpaired two-tailed t test, $N = 6$ to 7 per group) (fig. S13, A and B, and table S2). However, unlike Gapmer2, Arl5b mRNA levels were unchanged (shADEPTR versus shNC: $P = 0.31$ and shADEPTR + FSK versus shNC + FSK: $P = 0.25$, unpaired two-tailed t test, $N = 6$ to 7 per group) (fig. S13, A and B, and table S2). By imaging forskolin or DMSO-treated neurons expressing the shRNA or scrambled shRNA plasmid and performing spine analysis, we confirmed that ADEPTR knockdown suppresses cAMP-dependent changes in total (shNC + FSK: 68.63 ± 3.75, shNC + DMSO: 48.49 ± 5.2, and shADEPTR + FSK: 46.65 ± 4.28, $P < 0.001$, one-way ANOVA and Tukey's post hoc test) and mushroom spine density (shNC + FSK: 50.47 ± 3.77, shNC + DMSO: 31.08 ± 3.24, and shADEPTR + FSK: 32.1 ± 4.35, $P < 0.01$, one-way ANOVA and Tukey's post hoc test, $N = 19$ to 31 neurons per group) (fig. S13, C and D, and table S2). These data indicate that ADEPTR mediates activity-dependent changes in synaptic transmission and structural plasticity of dendritic spines.

ADEPTR is required for transient structural plasticity in stimulated spines

Given that ADEPTR mediates activity-dependent structural plasticity of dendritic spines and is transported to synapses, we hypothesized that ADEPTR specifically mediates the activity-dependent growth of stimulated spines. To test this hypothesis, we used glutamate uncaging using two-photon (2p) excitation in organotypic hippocampal slice cultures (Fig. 3A) (*27*). We used two independent shRNAs targeting ADEPTR, corresponding to Gapmer1 and Gapmer2 sequences, respectively, as well as a scrambled shRNA control. Neither shRNA targeting ADEPTR influenced immediate spine enlargement of uncaged spines at 0 to 70 s after uncaging

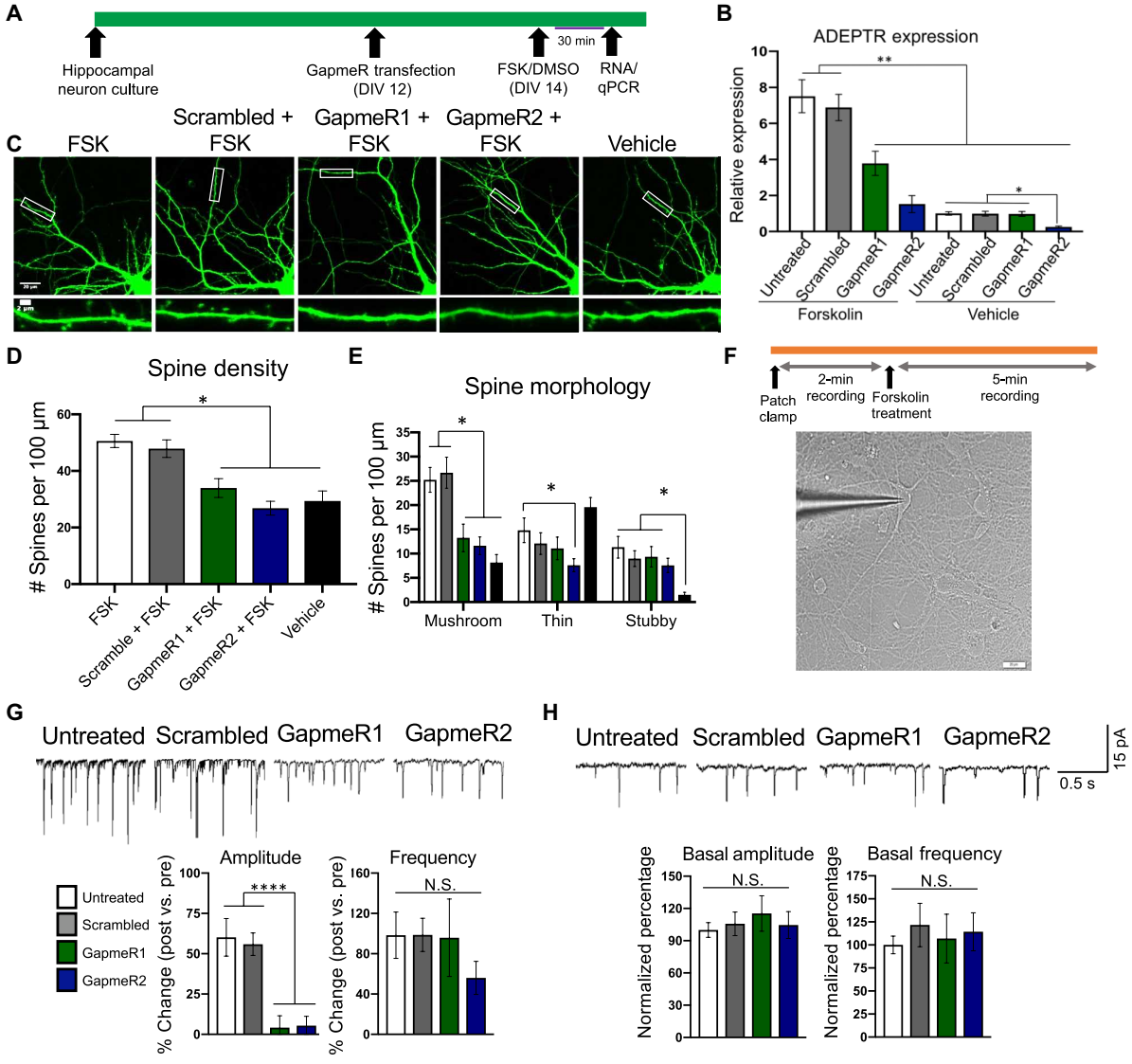

Fig. 2. ADEPTR expression is required for cAMP-dependent changes in dendritic spine dynamics and synaptic transmission. (**A**) Experimental timeline of transfection for gene expression measurement. (**B**) qRT-PCR measuring ADEPTR expression in forskolin or DMSO-treated hippocampal neurons after ADEPTR knockdown by two independent Gapmers. $N = 4$ to 6 independent wells per group. Error bars represent SEM. $^{*}P < 0.05$ and $^{**}P < 0.01$. One-way ANOVA and Tukey's post hoc test. (**C**) GFP-labeled/Gapmer-transfected cells were treated with forskolin or DMSO for 30 min and subjected to live imaging. (**D**) Analysis of spine density and (**E**) morphology as performed by MATLAB custom script. (**F**) Top: Timeline of transfection for electrophysiology experiments. Bottom: Representative image of a patched neuron for sEPSCs recording in the voltage-clamp mode. Forskolin was added to the bath at a final concentration of 25 µM. Scale bar, 20 µm. Analysis of amplitude and frequency from activity dependent (**G**) and basal (**H**) sEPSCs. $N = 22$ to 28 neurons per group from three independent experiments. In all graphs, error bars represent SEM. $^{**}P < 0.01$ and $^{****}P < 0.0001$, one-way ANOVA and Tukey's post hoc test.

(Fig. 3, B and C, and table S3). However, both ADEPTR-targeting shRNAs resulted in a transient reduction in dendritic spine size within 6.5 min of uncaging (1.5 to 3.5 min: shNC: 150 ± 15.5%, sh1: 107 ± 14.72%, and sh2: 70 ± 8.97%; 4.5 to 6.5 min: shNC: 104 ± 18.7%, sh1: 55.1 ± 12.1%, and sh2: 51.94 ± 8.3%, $P < 0.05$, one-way ANOVA and Dunnett's test, $N = 16$ to 18 spines from four to seven neurons per group) (Fig. 3, D and E, and table S3). There was no difference in sustained spine size by 20 min after uncaging between groups (Fig. 3, E and F, and table S3). Together, these results suggest that ADEPTR expression is critical to structural plasticity changes associated with stimulated dendritic spines.

Activity-dependent dendritic localization of ADEPTR is mediated by Kif2a

Given that ADEPTR is distally transported during cAMP signaling and mediates neuronal cAMP-dependent changes in structural plasticity, we hypothesized that ADEPTR might carry out its function at or near the site of plasticity changes through binding partners. To test this hypothesis, we performed an RNA antisense purification (RAP) to pull down ADEPTR from forskolin-treated hippocampal neurons (fig. S14A) and analyzed protein and RNA interactors. This protocol involved the use of two long [~300 to 400 nucleotides (nt)] antisense probes on the 5′ and 3′ end of the

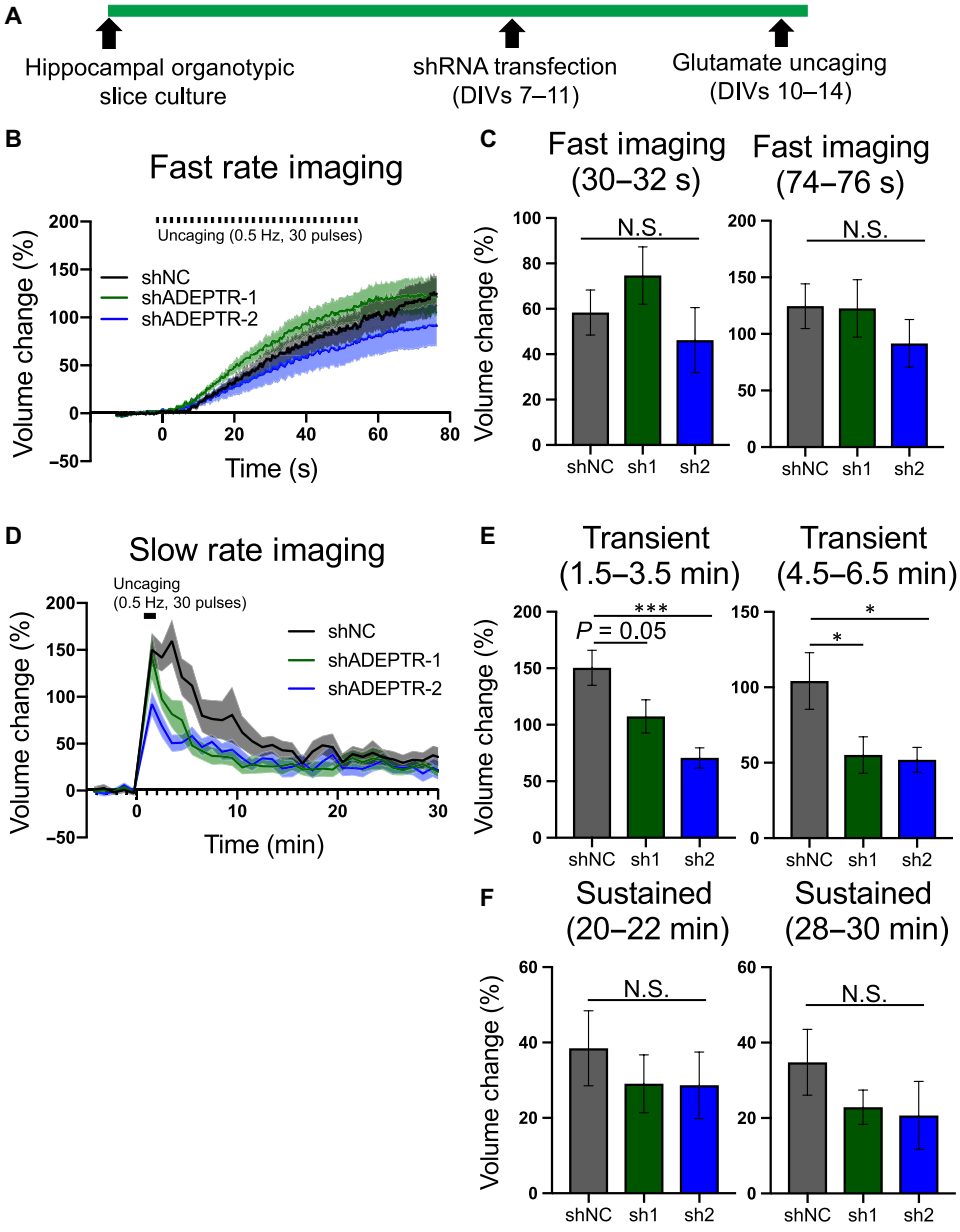

Fig. 3. ADEPTR is required for transient structural plasticity in stimulated spines. (**A**) Experimental timeline of hippocampal organotypic slice culture and shRNA transfection for glutamate uncaging experiments. (**B** and **C**) analysis of rapid spine volume changes up to 1.5 min after uncaging. (**D**) Analysis of transient and sustained spine volume changes 1.5 to 30 min after uncaging. (**E**) Analysis of discrete time bins in the transient and (**F**) sustained phase of glutamate uncaging. *$P < 0.05$ and ***$P < 0.001$, one-way ANOVA, followed by Dunnett's test, $N = 16$ to 18 spines from four to seven neurons per group.

putative ADEPTR transcript that sparsely contain biotin-incorporated uracils for streptavidin-based pulldown (fig. S14B). Sense probes were also implemented to control for nonspecific binding. qRT-PCR analysis showed that the RAP protocol robustly and specifically enriched ADEPTR (fold change 21.75 ± 3.07 relative to sense control, $N = 5$ to 8 per group, $P < 0.05$, unpaired two-tailed t test). Notably, neither Arl5b nor actin mRNA was preferentially enriched, indicating that the RAP protocol is specific to ADEPTR enrichment (fig. S14C).

We first examined the protein component of ADEPTR pulldown complexes and searched for molecular motors that might mediate ADEPTR localization. Using liquid chromatography–tandem mass spectrometry (LC-MS/MS) analysis, we identified a unique protein enriched in the ADEPTR RAP complex: kinesin motor Kif2a (Fig 4A). We validated this interaction through repeated independent pulldown experiments via Western blotting ($N = 4$ to 7 per group from three experiments, $P < 0.05$, one-way ANOVA and Tukey's post hoc test) (Fig 4B). As an additional control, we also incorporated proteins enriched in Malat1 RAP complexes. Given that Kif2a is part of the kinesin family of motor proteins responsible for anterograde transport, we hypothesized that Kif2a mediates ADEPTR transport. To test this hypothesis, we knocked down

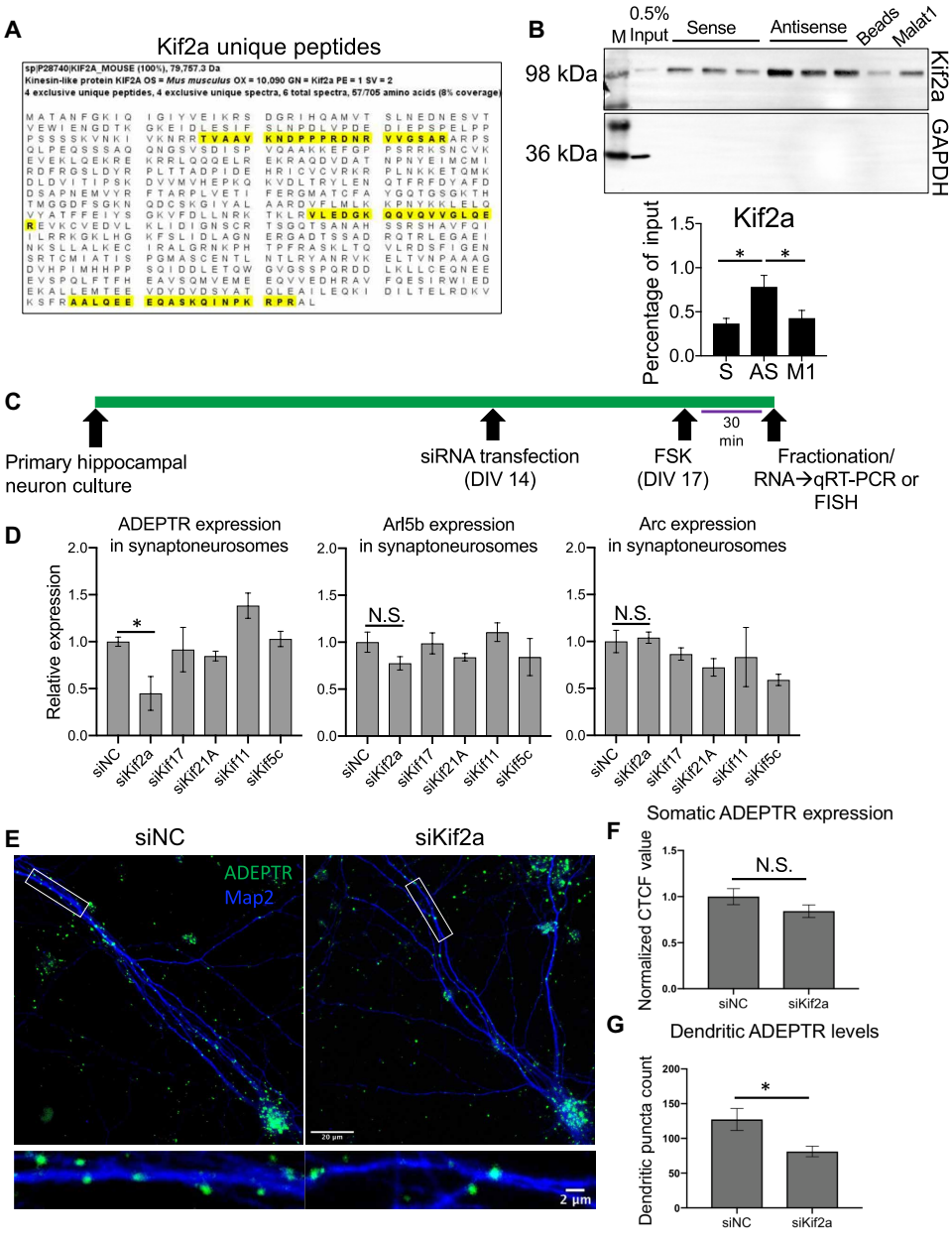

Fig. 4. Activity-dependent ADEPTR transport is mediated by Kif2a. (**A**) Top: Unique peptide counts of Kif2a from ADEPTR antisense purification, identified by LC-MS/MS. Bottom: Sequence coverage, percent chance of correct protein identification, and number of unique peptides and spectra. (**B**) Top: Western blotting of ADEPTR pulldown. Sense probes (S), beads alone, and Malat1 (M1) were used as controls. Bottom: Quantification of Western blotting based on percentage of input. $N = 4$ to 7 per group from three experiments. *$P < 0.05$, one-way ANOVA and Tukey's post hoc test. (**C**) Timeline for RNA interference (RNAi)–mediated knockdown of candidate kinesins for fractionation or FISH studies. (**D**) Neurons were treated with forskolin before fractionation and synaptosome RNA extraction. Graph shows qRT-PCR analysis of ADEPTR, Arl5b, and Arc expression in Kif2a, Kif17, Kif21A, Kif11, and Kif5c siRNA groups, relative to control. $N = 3$ to 4 independent wells per group. *$P < 0.05$, Dunnett's test. (**E**) FISH images from siKif2a + FSK or siNC + FSK. (**F**) Quantification of somatic and (**G**) dendritic ADEPTR expression. $N = 25$ to 28 neurons per group from three independent experiments. *$P < 0.05$, Student's t test. Error bars represent SEM. Scale bar, 20 µm (neuron image) and 2 µm (inset).

Kif2a, or four other kinesins, using small interfering RNAs (siRNAs) that were previously validated in hippocampal neurons for knockdown efficiency (*28*). Following 72 hours of knockdown, we treated neurons with forskolin before synaptoneurosome fractionation or ADEPTR FISH (Fig. 4C). qRT-PCR analysis from synaptosomes showed that Kif2a siRNA significantly down-regulated ADEPTR expression in synaptoneurosomes relative to scrambled siRNA (ADEPTR fold change in siKif2a relative to siNC: 0.45 ± 0.18, $N = 3$ to 4 per group; $P < 0.05$, Dunnett's test). Knockdown of Kif17, Kif21a, Kif11, and Kif5c did not show a concomitant decrease in ADEPTR expression. In addition, Arl5b and Arc mRNA expression in synaptosomes were not affected by any siRNA tested (Fig. 4D and table S4). We then repeated Kif2a knockdown and measured ADEPTR expression using FISH (Fig. 4E). While the somatic

fluorescence intensity of the ADEPTR channel was not significantly affected (Fig. 4F), the dendritic puncta account was significantly reduced, although not entirely suppressed, in Kif2a deficient neurons (siNC: 127.28 ± 15.8 and siKif2a: 81.14 ± 7.52, $N = 25$ to 28 neurons per group from three independent experiments, $P < 0.05$, Welch t test) (Fig. 4G and table S4). Together, these results show that activity-dependent dendritic localization of ADEPTR is mediated by Kif2a.

ADEPTR interacts with the spectrin/ankyrin complex and regulates their distal localization

LC-MS/MS analysis of ADEPTR RAP identified two additional associated proteins: spectrin-alpha-2 (Sptn1) and ankyrin-B (AnkB). We validated this interaction through independent pulldown experiments via Western blotting (AnkB and Sptn1: $P < 0.05$, one-way ANOVA and Tukey's post hoc test, $N = 4$ to 7 replicates from three experiments) (Fig. 5, A and B, and table S5).

Given that ADEPTR regulates activity-dependent spine changes in mature hippocampal neurons, we asked whether ADEPTR might regulate components of the spectrin/ankyrin network. Therefore, we globally knocked down ADEPTR in hippocampal neurons using a lentivirus expressing ADEPTR shRNA or control and isolated protein from synaptoneurosomes after treating neurons with forskolin or DMSO (Fig. 5C). We found, by Western blotting, that both Sptn1 and AnkB protein expression in synaptoneurosomes is up-regulated by cAMP signaling. AnkB, but not Sptn1, expression was reduced in ADEPTR-deficient neurons, in a cAMP-dependent manner in synaptoneurosomes (AnkB: shNC + FSK versus shADEPTR + FSK: $P < 0.01$, two-way ANOVA and Tukey's post hoc test, $N = 4$ to 6 per group) (Fig. 5, D and E, and table S5). Further, actin protein levels were not affected by either FSK treatment or ADEPTR knockdown (Fig. 5, D and E).

To better understand the role of ADEPTR in AnkB and Sptn1 expression in neuronal distal processes, we sparsely labeled neurons with the shRNA plasmid and performed super-resolution imaging of GFP-labeled distal neuronal processes immunostained with AnkB or Sptn1 under cAMP conditions (Fig. 5F). Structured illumination microscopy of distal neuronal processes confirmed that ADEPTR knockdown suppresses the dendritic localization of AnkB and Sptn1 only under cAMP conditions (AnkB and Sptn1: shNC + FSK versus shADEPTR + FSK, $P < 0.05$, two-way ANOVA and Tukey's post hoc test, $N = 30$ to 38 dendrite sections from 16 to 22 neurons from three experiments) (Fig. 5, G and H, and table S5). These results indicate that ADEPTR mediates dendritic localization of AnkB and Sptn1 thereby facilitating structural changes at the synapse.

ADEPTR interacts with AnkB and Sptn1 via a 222-nt fragment

We then asked what regions of ADEPTR are directly involved with protein binding. To address this question, we used a modified version of the RAP strategy that draws from elements of ribosome footprinting (*29*) and has previously been used to study lncRNA interactions (*30*). Briefly, forskolin-treated mature hippocampal neurons were chemically cross-linked, lysed, and sonicated. Upon pulldown of ADEPTR, unprotected regions of ADEPTR in the RAP complex were broken down by ribonuclease (RNase) treatment and separated from the protected fragments bound by protein using sucrose-cushioned ultracentrifugation. The RNase-protected RNA in the precipitate was then isolated for further analysis (Fig. 6A). Compared to the sense probe control, the RNA profile of the RNase-protected ADEPTR RAP complex showed a more robust distribution of peaks that concentrated in the 100- to 400-nt range (fig. S14D). We then performed RNA-seq and mapped the reads to the ADEPTR locus. Unexpectedly, we identified one predominant fragment at the 3′ end of the putative transcript that had a length of 222 nt (Fig. 6B). We then performed a pulldown from hippocampal neuron lysates using biotinylated oligo probes of an extended version of this sequence (positions 2415 to 2700 of the putative ADEPTR) or previously used sense probe (1924 to 2221) (Fig. 6C). Beads alone were used as a control for background levels of enrichment. We found that this sequence is sufficient to enrich AnkB and Sptn1, but not actin or glyceraldehyde-3-phosphate dehydrogenase (GAPDH), suggesting that this sequence is sufficient to pull down the AnkB and Sptn1 (AnkB: 2415 to 2700 versus beads: $P < 0.01$ and Sptn1: 2415 to 2700 versus beads: $P < 0.05$, one-way ANOVA and Dunnett's test compared to beads, $N = 3$ to 5 replicates from three experiments) (Fig. 6, D and E, and table S6).

ADEPTR directly interacts with the ankyrin/spectrin network via a 32-nt sequence found in several human mRNA 3′UTRs

Cross-referencing the 222-nt fragment with known features of the mouse reference genome, we found that it contains multiple conserved regions, as well as a short-interspersed nuclear element (SINE) (Fig. 7A). We then performed BLAST analysis on this fragment to the human genome and noted a ~32-nt region that mapped to multiple human mRNAs—most strongly to the negative transcription elongation factor NELFCD, peroxisome biogenesis factor PEX26, cation channel subunit TRPC3, and the glycosylphosphatidylinositol anchor protein PIGT. Notably, for all mRNAs analyzed by E value thresholding, this region was shown to reside within their 3′UTRs (Fig. 7B). We hypothesized that this fragment within ADEPTR is specifically responsible for directly binding of Sptn1, AnkB, or both. Therefore, we prepared three separate constructs for generating biotinylated probes: an 837-nt sequence corresponding to the 3′ end of the putative ADEPTR sequence (WT), the same construct lacking the 32-nt binding region (Del), and one containing the reverse complement of the binding region (Sub) (Fig. 7C). Western blotting of pulldowns from hippocampal neuron extracts showed that the WT fragment had a significantly higher enrichment of both AnkB and Sptn1 compared to beads alone, while neither the Del nor Sub fragments had a significant enrichment of these proteins (AnkB and Sptn1: WT versus beads: $P < 0.001$, one-way ANOVA and Dunnett's test, $N = 3$ replicates from two experiments) (Fig. 7, D and E, and table S7). Actin and GAPDH were not preferentially enriched in any pulldown condition.

Last, to confirm the significance of this conserved region in binding to protein via an alternative strategy, we asked whether the 32-nt fragment alone could interact with proteins. Therefore, we performed an RNA electrophoretic mobility shift assay (EMSA) on hippocampal neuron extracts using 3′ end biotinylated conserved 32-nt RNA sequence (Oligo1) of ADEPTR, the same construct with a single-point mutation ($_{SNP}$Oligo1), an alternative region of ADEPTR (Oligo2), or iron-responsive element (IRE) control RNA. We observed that protein extracts from hippocampal neurons bind Oligo1 better than the other three RNAs tested (fig. S15A), suggesting functional interactions of the conserved 32-nt region. We then performed a pulldown experiment using the short oligos (Oligo1, $_{SNP}$Oligo1, and Oligo2; fig. S15). We included an additional control

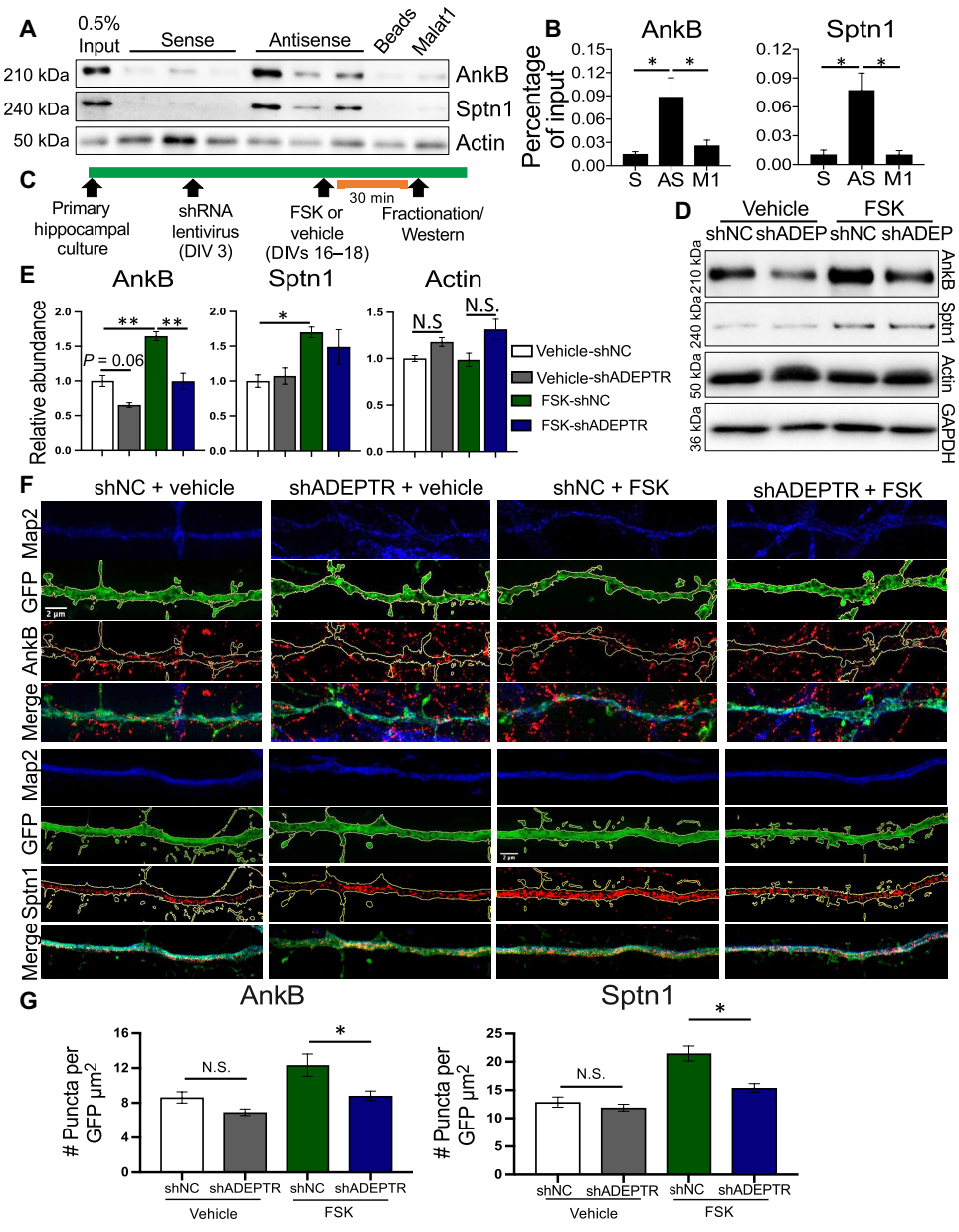

Fig. 5. ADEPTR binds to Sptn1 and AnkB and regulates their activity-dependent dendritic localization in hippocampal neurons. (**A**) Western blotting of ADEPTR antisense purification. Sense probes (S), beads alone, and Malat1 (M1) were used as controls. (**B**) Quantification of Western blotting based on percentage of input. $N = 4$ to 7 per group from three experiments. *$P < 0.05$, one-way ANOVA and Tukey's post hoc test. (**C**) Timeline for RNAi-mediated lentiviral knockdown of ADEPTR for synaptoneurosome fractionation studies. (**D**) Western blotting of indicated proteins in synaptoneurosome fractions. (**E**) Quantification of AnkB, Sptn1, and actin expression in synaptoneurosomes, $N = 4$ to 6 independent reactions per group from three experiments. *$P < 0.05$ and ***$P < 0.001$, two-way ANOVA and Tukey's post hoc test. (**F**) Top: Structured Illumination Microscopy images of AnkB and (bottom) Sptn1 within GFP-labeled neuronal processes from shNC or shADEPTR expressing FSK-treated neurons. Scale bar, 2 µm. (**G**) Quantification of respective protein puncta. $N = 30$ to 38 dendrite sections from 16 to 22 neurons per group. *$P < 0.05$, two-way ANOVA and Tukey's post hoc test. Error bars represent SEM.

oligo corresponding to a 5′ region of ADEPTR (Oligo3). There was no preferential interaction with Sptn1 suggesting that this 32-nt fragment alone is not sufficient to pull down the complex ($N = 3$ to 4 per group, $P = 0.34$, one-way ANOVA) (fig. S15B and table S7). Together, these data show that ADEPTR directly interacts with the ankyrin/spectrin network via a 32-nt repeat element that is also found in 3′UTRs of few human mRNAs.

DISCUSSION

Synaptically localized RNAs are an important component of neuronal function and cognitive processes such as long-term memory (*31*) but much less is known about the identity of noncoding components, regulation of their localization, and function. Previous works have attempted to unearth the synaptic transcriptome through multiple approaches, such as kinesin immunoprecipitation

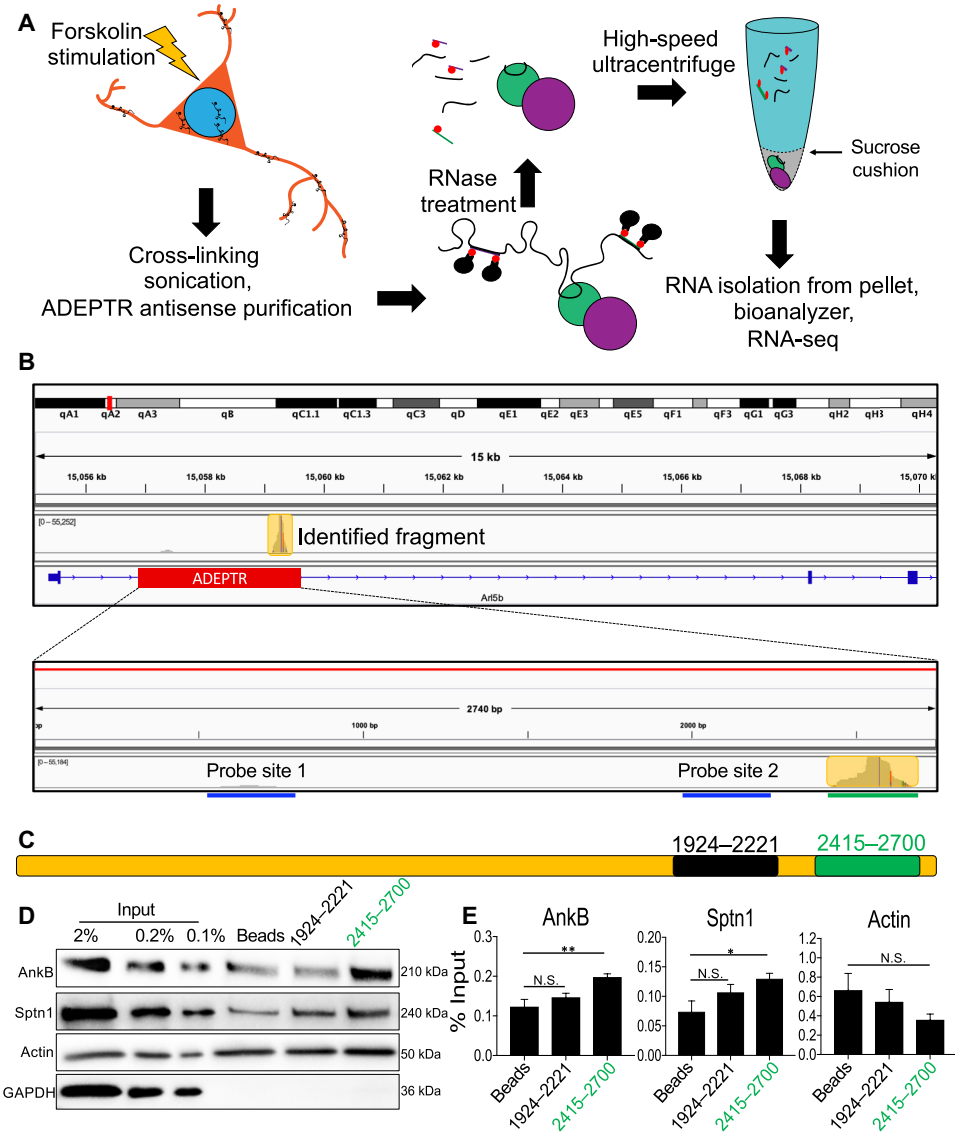

Fig. 6. Identification of protein binding sequences of ADEPTR. (**A**) Schematic summarizing the strategy to pull down ADEPTR under cross-linked conditions, purify the protected regions using RNase treatment and ultracentrifugation under sucrose gradient, and identify the fragments by RNA-seq. (**B**) Reads were mapped to the mouse genome using STAR and transcriptome using Salmon and visualized on Integrative Genomics Viewer software. (**C**) Schematic of regions of ADEPTR used for making sense probes. Green probe represents the conserved domain, and black probe represents the same sense probe control used in Figs. 4 and 5. (**D**) Western blotting and (**E**) quantification of RNA pulldowns using the ADEPTR fragments. $N = 3$ to 5 independent reactions per group from three experiments. $^*P < 0.05$ and $^{**}P < 0.01$, one-way ANOVA and Tukey's post hoc test. Error bars represent SEM.

(*32*), neurite sectioning (*33*, *34*), and synaptosome fractionation (*35*), coupled with microarray or RNA-seq. Our analyses, combining next generation RNA-seq, qRT-PCR, FISH, and nascent RNA capture have identified a novel noncoding RNA transcript—ADEPTR—as an intronic lncRNA that is synaptically targeted in a cAMP-dependent manner, independent of its protein-coding host gene. Through pharmacology screening, we identified that ADEPTR is specifically regulated by excitatory signaling, and unlike Arl5b, its cAMP-induced expression is dependent on the activity of PKA. In addition, ADEPTR and Arc—but not Arl5b— expression are negatively regulated by GABA exposure. Collectively, these results suggest that ADEPTR is up-regulated by cAMP-PKA signaling and down-regulated by GABA signaling.

It has been previously reported that functional intronic lncRNAs can be utilized as retained introns within mRNAs (*36*, *37*), excised products from pre-mRNAs (*38*, *39*), and as stable sequences with independent transcription (*40*). In addition, intronic lncRNAs can be atypically processed into a circular confirmation (*39*) or contain small nucleolar RNA (snoRNA) ends (*41*). Our work has identified a novel type of lncRNA that is independently expressed and distally transported to neuronal synapses.

Loss-of-function experiments, using locked nucleic acid (LNA) Gapmers and shRNAs, have established that this lncRNA is necessary for cAMP-dependent structural plasticity of dendritic spines in hippocampal neurons. This deficiency largely occurred in the mushroom spines, indicating that ADEPTR specifically regulates potentiated spines

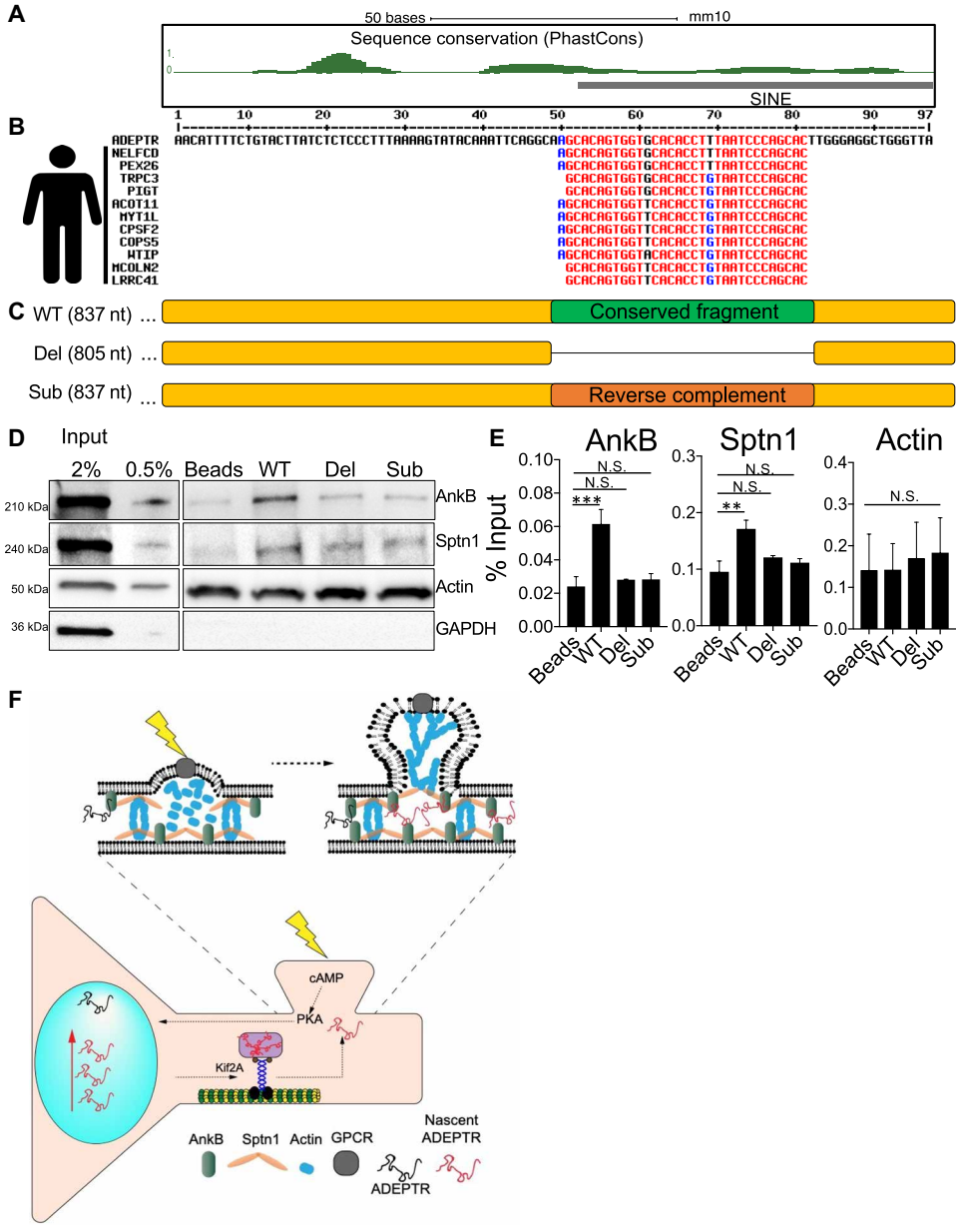

Fig. 7. ADEPTR directly interacts with the ankyrin/spectrin network via a conserved domain found in human mRNA 3′UTRs. (**A**) The fragment identified was mapped to University of California Santa Cruz genome browser and analyzed for conservation (PhastCons) and presence of repeat elements (RepeatMasker). (**B**) A 97-nt region showing the highest conservation was blasted to the human cDNA reference using Ensembl, and top hits (*E* value < 0.001) were aligned using MultAlin. Mapping to each human mRNA 3′UTR was performed using Ensembl BioMart. (**C**) Schematic of biotin-labeled fragments of ADEPTR containing the conserved region, a deletion, or substitution. (**D**) Western blotting and (**E**) quantification of RNA pulldowns using the ADEPTR fragments shown in (**C**). $N = 3$ independent reactions per group from two experiments. $^{**}P < 0.01$ and $^{***}P < 0.001$, one-way ANOVA and Tukey's post hoc test. Error bars represent SEM. (**F**) Proposed model for ADEPTR in mediating structural plasticity.

during neuronal activation. However, overall dendritic morphology is not affected. Supporting electrophysiology experiments showed that ADEPTR does not influence synaptic transmission under basal conditions but rather specifically mediates cAMP-dependent changes in EPSC amplitude. Furthermore, glutamate uncaging experiments showed that ADEPTR is required for activity-dependent transient spine enlargement specifically at stimulated spines. These results suggest that ADEPTR affects both the activity-dependent increase in number of mushroom spines, as well as the transient increase in size of existing mushroom spines. Given that only the transient, but not sustained, spine size was affected with ADEPTR knockdown, this suggests that alternate compensatory mechanisms may initiate during the transient phase of structural plasticity to recover from the effects of ADEPTR deficiency. Furthermore, the complete functional significance of ADEPTR impact on transient plasticity remains to be elucidated, given that the exact

physiological role of the transient phase of structural plasticity is unknown (*7*). Previous work has established that Rac1 and RhoA are involved in the transient changes in spine size (*7*); further study should elucidate whether ADEPTR acts with these proteins, either directly or through its interacting partners.

Although previously identified lncRNAs have shown an influence in basal hippocampal neuron function—these include Malat1, NeuroLnc, NEAT1, and Gm12371 (*11*, *42*–*44*)—none of these lncRNAs are targeted to synapses in an activity-dependent manner for regulating spine dynamics. Given the discrete expression pattern of ADEPTR under cAMP signaling, our results suggest that ADEPTR plays a defined yet potent role in activity-dependent structural plasticity (see Fig. 7F).

We further found that ADEPTR localizes in dendrites at discrete distal positions in a cAMP-dependent mannner. Particularly, we found through nascent RNA extraction from synaptoneurosomes as well as inhibition of transcription by actinomycin D that ADEPTR is distally localized as a nascent RNA. We next found that the distal localization, but not the expression, of ADEPTR is dependent on microtubule and actin polymerization. This suggested that ADEPTR is being actively trafficked by canonical transport mechanisms, of which kinesins play a major role. In line with this observation, we have uncovered a specific kinesin motor—Kif2a—as a binding partner and mediator of ADEPTR distal transport. Kif2a is an M-terminal kinesin and, since its discovery, has been shown to carry cargoes in neurons (*45*, *46*). It has also been shown to function as a microtubule destabilizer, regulating neuronal outgrowth (*47*). However, its microtubule destabilizing function can be inhibited by BDNF signaling, suggesting the possibility of a dual role for this protein that is regulated by activity (*47*). Future study will require a deeper molecular understanding of how different converging signaling pathways result in Kif2a-dependent distal localization of ADEPTR and other potential cargoes.

We then showed that ADEPTR binds to the spectrin/ankyrin network, specifically Sptn1 and AnkB. It is known that early to mid-stage plasticity changes are mediated by post translational activities such as protein-dependent signaling cascades resulting in cytoskeletal rearrangements (*48*). Sptn1 is a filamentous protein that interacts with its complementary β subunit to scaffold the actin cytoskeleton (*49*). It exhibits a unique pattern of periodicity in neuronal processes that complements periodic actin (*50*, *51*). Spectrin is anchored to the plasma membrane through ankyrin proteins. AnkB (Ank2) is a brain-enriched ankyrin member that is expressed in both axons and dendrites (*52*). Together, the spectrin/ankyrin complex has been known to be required for actin-enriched spine formation (*53*) and neurite assembly (*54*). Sptn1 and AnkB were also shown to interact in neurons to stabilize the T-type calcium channel Cav3.2 (*55*). However, it remains unresolved how this network is regulated in neurons. We have demonstrated that the interaction of ADEPTR with the Sptn1/AnkB network is functional as its expression is necessary for the cAMP-dependent localization of AnkB in synaptoneurosomes and both AnkB and Sptn1 in dendritic processes.

RNase-protection experiments showed that a 222-nt fragment is uniquely protected by RNase treatment, suggesting that it may bind protein. Pulldown experiments confirmed that this 222-nt fragment of ADEPTR is sufficient to enrich AnkB and Sptn1. Previously discovered lncRNAs have been shown to interact with proteins with no defined RNA-binding capabilities, through protected domains (*40*, *56*), demonstrating an intriguing capability of regulatory RNAs typically ascribed to proteins. Here, we found that the interaction within this protected 222-nt region is through a 32-nt region that overlaps SINE B1 domain, found in 3′UTRs of human mRNAs. Pulldown experiments using the 3′ end region of ADEPTR containing either a mutation or a deletion of this 32-nt fragment showed that this sequence is necessary to enrich the Sptn1/AnkB complex, suggesting that this region is protected via its interaction with Sptn1/AnkB. However, while this 32-nt fragment alone showed unique interactions with proteins in the EMSA experiments, this fragment is not sufficient to pull down Sptn1. This suggests that the context of the lncRNA secondary structure determines the binding the Sptn1/AnkB complex. It has previously been shown that lncRNA functions in the cytoplasm of dopaminergic neurons through a SINE Alu repeat to salvage the expression of an mRNA (*30*), although the functional consequence of this rescue in neurons warrants further study. Furthermore, a brain-enriched zebrafish lncRNA lacking direct homologs in higher organisms has previously been shown to regulate zebrafish behavior via interaction with miR-29. Its miRNA interaction site is conserved in the 3′UTR of an mRNA in mice and humans (*57*).

Computational analysis has drawn parallels between lncRNAs and 3′UTRs in terms of structural features and sequence composition, namely, that they have similarly low protein-coding potentials, have a low GC content, and show a less stable secondary structure compared to that of open reading frames and even 5′UTRs. These suggest that both lncRNAs and 3′UTRs are more reliant on protein interactions for their stability than mRNAs (*58*). In line with these discoveries, our findings show that ADEPTR functions in the cytoplasm through cytoskeletal-regulating proteins AnkB and Sptn1 and is subsequently turned over. The identification of a conserved functional region of ADEPTR that matches to multiple human mRNA 3′UTRs is further evidence that noncoding elements—even within protein-coding genes—can play a role in structural plasticity. ADEPTR activity seems to fit this pattern of regulation and may put fourth an intriguing role for lncRNAs locally regulating sites of structural plasticity.

Although ankyrin is a canonical binding partner of spectrin subunits, the precise mechanism of how these proteins regulate structural plasticity remains to be elucidated. AnkB is known to bind a multitude of distal targets including the plasma membrane, different spectrin isoforms, L1-CAMs and calcium channels (*37*, *38*). Given the previously established role for AnkB in regulating voltage-gated calcium channels in dendrites (*55*), it is possible that by scaffolding AnkB, ADEPTR is indirectly involved in mediating calcium influx for activity-dependent remodeling of synapses.

lncRNAs are emerging as subtle yet powerful regulators of gene expression and cellular function, and their subcellular localization is an important indicator of their function. Akin to previously studied lncRNAs (*59*), ADEPTR shows both a nuclear and somatic expression upon activity, thereby raising an important question as to how it carries out its phenotype. Given the rapid expression and shuttling of ADEPTR to distal processes, as well as the interaction with structural proteins Sptn1 and AnkB, our results suggest that ADEPTR carries out its function predominantly in the distal cytoplasm. Cytoplasmic lncRNAs have also been demonstrated to act as scaffolds for protein complexes: a role also attributed to UTRs or noncoding isoforms of mRNAs (*60*–*62*).

Ultimately, our study describes a cAMP/PKA-dependent lncRNA that is expressed, distally transported by a kinesin motor protein, and regulates structural plasticity through functional interactions with the spectrin/ankyrin network. This study illuminates our understanding of noncoding elements of the synaptically targeted transcriptome, of which we know very little, and puts forth synaptically localized lncRNAs as important regulators of adaptive neuronal function.

MATERIALS AND METHODS

Animals

CD1 pregnant mice (Charles River Laboratories) were housed individually on a light-dark (12-hour/12-hour) cycle with ad libitum access to food and water. Experiments were performed during the light part of the diurnal cycle. Housing, animal care, and experimental procedures were consistent with the *Guide for the Care and Use of Laboratory Animals* and approved by the Institutional Animal Care and Use Committee of The Scripps Research Institute.

Primary hippocampal neuron culture

Hippocampi were dissected from E18 CD1 pups and plated on poly-D-lysine–coated plates in Neurobasal medium supplemented with GlutaMAX (Thermo Fisher Scientific, 35050061), penicillin-streptomycin (10,000 U/ml) (Life Technologies, 15140-122), and 5% fetal bovine serum (Thermo Fisher Scientific, 16000044). Density of neurons plated was varied by experimental requirement. For neurons plated in six-well plates (used in RNA-seq, qPCR, and RNA pulldown experiments), the plating density was 500,000 cells per well. For imaging experiments (FISH and Immunocytochemistry), the cells were plated on poly-D-lysine–coated glass coverslips (24-well plate format) at a concentration of 80,000 to 100,000 cells per coverslips. For imaging experiments involving plasmid transfection or virus transduction, the cells were plated in a 24-well plate format at 150,000 cells per well. Four hours after plating, medium was replaced with feeding medium consisting of Neurobasal medium supplemented with GlutaMAX, penicillin-streptomycin, and 2% B27 (Thermo Fisher Scientific, 17504044), and half of the medium was replaced every 4 days until the time of experiments at 37°C with 5% CO_2.

Transfection of plasmid constructs, LNA Gapmers, and siRNAs

GFP reporter plasmids (enhanced GFP and PLL3.7 shRNA) were transfected into neurons at day in vitro (DIV) 14 using Lipofectamine 2000 (Invitrogen, 11668019). LNA Gapmers targeting ADEPTR or siRNAs targeting kinesins were transfected using Lipofectamine RNAiMax (Invitrogen, 13778075). LNA Gapmers were synthesized by Exiqon (now Qiagen) and transfected as previously described (*15*). Briefly, siRNAs and Gapmers or shRNAs were introduced to primary hippocampal neurons (5 to 8 DIVs) using Lipofectamine RNAiMAX or Lipofectamine 2000 according to the manufacturer's guidelines. One day before transfection, the fresh culture medium was prepared and mixed evenly with the old medium. One-half of the mixed medium was added to the cells for transfection, and the other one-half was saved for medium replacement for transfection. The sequence for Gapmer1 targeting ADEPTR is as follows: 5′-TTAGGTGCCAGAATAA-3′, Gapmer2 targeting ADEPTR: 5′-TTTCCATCTTGCACCTAGCAG-3′, and scrambled Gapmer: 5′-AA CACGTCTATACGC-3′. siRNAs targeting kinesins were previously used in primary hippocampal neuron cultures and validated to have robust knockdown efficiency (*30*). For ADEPTR FISH experiments involving siRNAs (Fig. 4, E to G), we used data from three independent experiments ($N = 25$ to 28 neurons), to assess the effect of Kif2A knockdown on ADEPTR localization. The sequence for shRNA 1 and 2 cassettes for ADEPTR knockdown correspond to the Gapmer 1 and 2 sequences, respectively. Scrambled shRNA cassette: 5′-AGTTCCAGTACGGCTCCAA-3′.

Pharmacology

Additional pharmacological agents used on hippocampal neurons were PKA inhibitor 14 to 22 amide (2.5 μM, 30 min before FSK treatment), A2A receptor agonist adenophostin A (5 nM, 30 min), protein kinase C activator phorbol 12-myristate 13-acetate (1 μM, 30 min), D1 receptor agonist SKF38393 (10 μM, 30 min), L-glutamate (500 nM, 30 min), potassium chloride (50 mM, 30 min), TTX (μM, 30 min before FSK treatment), and GABA (5 μM, 30 min).

Cell fractionation

For synaptoneurosome preparation, DIV 16 to 18 hippocampal neurons were washed once with ice-cold phosphate-buffered saline (PBS) and lysed in Syn-PER Synaptic Protein Extraction Reagent (Thermo Fisher Scientific, PI87793), as per the manufacturer's instructions. For nuclear/cytoplasmic isolation, neurons were washed with cold PBS and lysed in cytoplasmic buffer [20 mM tris-HCl 20, 150 mM KCl, 1.5 mM $MgCl_2$, 1 mM dithiothreitol (DTT), 0.5% NP-40, and 1× EDTA-free protease and phosphatase inhibitor cocktails (Sigma-Aldrich, 11836170001, P0044, and P5726)] and gently centrifuged at 4°C to separate the nuclear fraction (pellet) from the cytoplasmic supernatant.

Transmission electron microscopy

Synaptoneurosome pellets were resuspended 2.5% glutaraldehyde (EM grade, 50% aqueous solution; Electron Microcopy Science) within 150 mM cacodylate buffer (pH 7.4) at 4°C overnight. Upon washing in buffer and then water, synaptoneurosomes were treated with 1% aqueous OsO_4 on ice for 1 hour, stained en bloc with 1% aqueous uranyl acetate for 1 hour, dehydrated with an ethanol and acetone series, and flat-embedded in Durcupan resin (Sigma-Aldrich). The samples were then polymerized at 60°C for 2 days and imaged on a Tecnai G2 Spirit BioTwin transmission electron microscope (FEI).

Quantitative real-time PCR

RNA was isolated using TRIzol and reversed transcribed into cDNA using qScript cDNA SuperMix (Quantabio, 101414-106). qRT-PCR was performed in 384-well plates using SYBR Green Master Mix (Applied Biosystems) for detection in the ABI 7900 thermal cycler (Applied Biosystems). ΔC_T values were obtained using C_T values for 18 s for normalization, followed by relative quantification using $2^{-\Delta CT}$ method.

RNA-seq and analysis

Total RNA-seq was performed following the Scripps Florida Genomics core protocol, as described previously (*11*). Fastq files were first assessed for quality using fastqc and trimmed using Trim Galore on the Scripps high-performance computer cluster. Fastq reads were then aligned to the *Mus musculus* transcriptome using Salmon (*63*), also using Scripps high-performance computing cluster, to generate raw counts and transcripts per million data based on Ensembl Transcript

IDs. Data were then imported into R using tximport Bioconductor package and clustered using clusterProfiler. Differential expression analysis was performed using DEseq2. RNa-seq data are deposited to the National Center for Biotechnology Information (NCBI) Gene Expression Omnibus with the accession number GSE157388.

Nascent RNA capture

Nascent RNA capture was performed using the Click-iT Nascent RNA Capture Kit (Life Technologies, C10365) using the manufacturer's instructions. Primary hippocampal neurons were treated with 5-ethynyl uridine (5-EU) at DIV 16. Twenty-four hours later, neurons were treated with forskolin (50 μM) or DMSO (equal volume) for 30 min and then lysed in TRIzol for total RNA extraction. Ten percent of the total RNA was saved, while the remaining 90% was processed for click chemistry–based azide biotinylation of the 5-EU, followed by binding to MyOne Streptavidin T1 beads and elution.

RNA FISH and immunofluorescence

Two 300– to 400–base pair (bp) fragments of ADEPTR, Arl5b, and Malat1 cDNA were subcloned into PCRII TOPO vectors and in vitro–transcribed into digoxygenin (DIG)-labeled probes for FISH. Anti-DIG fab fragment antibody (Roche, 11207733910) was used at a concentration of 1:4000, and tyramide signal amplification (PerkinElmer, NEL744001KT) was used using the manufacturer's instructions. One of the fragments, targeting the 3′ end of ADEPTR, was more efficient at producing a robust signal and therefore was used for all subsequent studies. Immunofluorescence was performed in conjunction to or separate from FISH, according to the experiment. Antibodies include Map2 (Synaptic Systems, 188004), PSD-95 (Thermo Fisher Scientific, MA1-45), GFP (Abcam, ab13970), actin (Abcam, Ab8227), synaptophysin (Abcam, ab32594), ankyrin B (Santa Cruz Biotechnology, sc-12718), spectrin-1 (Santa Cruz Biotechnology, sc-53444). Samples were imaged on the Zeiss LSM 880 confocal microscope at the Max Planck Florida Institute light microscopy facility. Neurons were plated at a low density (80,000 cells per well of a 24-well plate) to allow for imaging of single neurons at a time, with minimal crossover from other neurons.

FISH puncta acquisition and analysis

To analyze dendritic RNA puncta count, for each neuron imaged, the Map2-labeled dendrites were traced in Fiji ImageJ [National Institutes of Health (NIH)], and FISH puncta were acquired using a custom ImageJ macros script. The puncta count per neuron and the size of each punctate (in microns) were exported into R for statistical analysis. The puncta sizes were divided into discrete bins in R, and the frequency per bin was quantified for each experiment.

Spine and Sholl analyses

Spine and Sholl analyses were performed as previously described (*11*). Briefly, GFP-expressing neurons were brought to the light microscopy facility at the Max Planck Florida Institute and imaged at room temperature using the Zeiss LSM 780 confocal microscope. Z stacks were acquired using Zen software (2015, 64 bit), and maximum intensity projections were obtained. Dendritic arbors were obtained and quantified using Sholl analysis in Fiji (ImageJ, NIH). Spine analysis was performed on secondary branches from basal and apical dendrites on the maximum intensity projection images, using a custom MATLAB script. Values were obtained for total, mushroom, thin, and stubby spine density per 100 μm.

Patch-clamp electrophysiology

Whole-cell patch-clamp recordings were performed as previously described (*11*). Briefly, primary hippocampal neurons at DIVs 9 to 12 were patched using Axon Multiclamp 700B amplifier, 1440A Digidata digitizer, and pClamp software (Axon Instruments, Foster City, CA). Current and voltage recordings were made at 50 kHz and subsequently filtered at 5 kHz. The recordings were conducted blindly with four groups: untransfected, scrambled LNA Gapmer, ADEPTR Gapmer1, and ADEPTR Gapmer2. sEPSCs were recorded before and after the bath application of forskolin under voltage clamp. The current clamp was recorded only to identify the health of the neurons. Only neurons with resting membrane potential of more than −40 mV were used for our analysis.

Organotypic hippocampal slice cultures and transfection

Organotypic hippocampal slices were prepared from wild-type postnatal 4- to 7-day-old mouse pups of both sexes as previously described (*64*). In brief, the animals were anesthetized with isoflurane, after which the animal was quickly decapitated and the brain removed. The hippocampi were dissected and cut into 350-μm-thick coronal hippocampal slices using a McIlwain tissue chopper (Ted Pella Inc.) and plated on hydrophilic polytetrafluoroethylene membranes (Millicell, Millipore) fed by culture medium containing minimum essential medium (Life Technologies), horse serum (20%), L-glutamine (1 mM), $CaCl_2$ (1 mM), $MgSO_4$ (2 mM), D-glucose (12.9 mM), $NaHCO_3$ (5.2 mM), Hepes (30 mM), ascorbic acid (0.075%), and insulin (1 μg/ml). Slices were incubated at 37°C in 5% CO_2. After 7 to 12 DIVs, CA1 pyramidal neurons were transfected with biolistic gene transfer using 1.6-μm gold beads (8 mg) coated with plasmids containing 50 μg of total cDNA of interest (*65*).

2p fluorescence microscopy and 2p glutamate uncaging

4-Methoxy-7-nitroindolinyl (MNI)–caged glutamate uncaging and time-lapse structural imaging of spines were performed using a custom-built 2p laser microscope as previously described (*66*). The 2p imaging and uncaging were performed using two Ti-sapphire lasers (Coherent, Cameleon) at wavelengths of 920 nm (1.45 to 1.55 mW under the objective) for imaging and 720 nm (2.7 to 3.0 mW under the objective) for uncaging. Green fluorescence emission was collected using an immersion objective (LUMPlan FL N 60×, numerical aperture 1.0, Olympus), reflected by a dichroic mirror (565-nm LP) and passed a filter (Chroma, 510 nm/70-2p) before entering the fast photoelectron multiplier tubes (H7422-40p; Hamamatsu). Fluorescence images were acquired and quantified using a TimeHarp 260 Pico card (PicoQuant Inc.) and a custom-built software, FLIMage (version 2.0.0) written with #C (https://github.com/ryoheiyasuda/FLIMage_public). Image acquisitions for monitoring long-term structural long-term potentiation (LTP) volume changes were collected by 128 × 128 pixels as a Z stack of five frames with 1-μm distance in each frame and averaging six scans per frame (frame rate, 0.65 Hz). Fast-rate simultaneous image acquisitions with uncaging were collected by 64 × 64 pixels at a single *z* plane without averaging per frame (frame rate, 7.8 Hz). MNI-caged L-glutamate (Tocris) was uncaged with a train of 8- to 10-ms laser pulses (under the objective, 30 times at 0.5 Hz) near a spine of interest. Experiments were performed at room temperature (24° to 26°C) in artificial cerebrospinal fluid solution containing: NaCl (127 mM), KCl (2.5 mM), $NaHCO_3$ (25 mM), NaH_2PO_4 (1.25 mM), $CaCl_2$ (4 mM), glucose (25 mM), TTX (1 μM), and 4-MNI-caged L-glutamate (4 mM), bubbled with

95% O_2 and 5% CO_2. We examined secondary or tertiary branches of apical dendrites of CA1 pyramidal neurons (located in stratum radiatum) in organotypic cultured hippocampus slices at 11 to 17 DIVs.

Statistical analysis for glutamate uncaging experiments

Spine volume change was calculated by F/F_0, in which F0 is the average spine intensity before stimulation. All values are presented as mean ± SEM unless otherwise noted. Number of independent measurements [*n* (spines/neurons)]. One-way ANOVA followed by Dunnett's test was used to compare grouped datasets (Prism 8.3, GraphPad). Data were excluded if signs of poor cellular health or procedural artifacts (for example, dendritic blebbing and displacement of dendrites) were apparent.

Native and cross-linked RAP

RAP was performed as previously described (*56*) with a few modifications. The day before experiments, streptavidin beads (New England Biolabs) were washed twice and blocked in pulldown buffer [tris-HCl 50 mM (pH 7.4), NaCl 150 mM, EDTA 0.5 M, NP-40 0.25%, 1% bovine serum albumin (BSA), DTT 1 mM, SUPERase RNase inhibitor, protease inhibitor (Roche), and phosphatase inhibitor cocktails (Roche)] supplemented with 4% BSA, 20 μM glycogen, and 20 μM yeast RNA (Thermo Fisher Scientific) overnight. On the day of experiments, DIV 15 to 18 primary hippocampal neurons were treated with forskolin (50 μM) for 30 min to boost the endogenous expression of ADEPTR and then lysed in a pulldown buffer. Cells were scraped and collected into Eppendorf tubes, rotated for 20 min at 4°C, and centrifuged at 1200*g* at 4°C for 20 min to pellet the debris. The supernatant was then collected and divided into 400-μl reactions. Biotinylated RNA probes were prepared just as in RNA FISH, using Biotin RNA Labeling Mix (Sigma-Aldrich). Before the experiments, probes were heated at 72°C, then kept once ice until added to reaction, and rotated at room temperature for 3 hours. The blocked streptavidin beads were washed an additional time and added to the reaction for an additional hour. After five stringency washes, the beads were resuspended with TRIzol for RNA extraction or Laemmli buffer for protein extraction.

For cross-linked RAP, neurons were washed in PBS and cross-linked with 4% paraformaldehyde for 15 min, followed by another PBS wash, and lastly, lysis buffer. Cells were scraped and pooled into one falcon tube for sonication (15 s on, 15 s off for 10 min) and gently centrifuged (1200*g*, 10 min, 4°C) to clear the debris. Supernatant was then subjected to pulldown as described above. Stringency washing was performed with pulldown buffer lacking BSA and an NaCl concentration of 600 mM. Beads were then resuspended with tris buffer containing RNase A (10 μg/μl), incubated at 37°C for 60 min, and pelleted. The supernatant was treated with SUPERase RNase inhibitor and transferred to an ultracentrifuge tube for ultracentrifugation (70,000 rpm, 4 hours, 4°C) with a 1 M sucrose gradient. The supernatant was then decanted, and the pellet was suspended in TRIzol for total RNA extraction, bioanalyzer measurements, and RNA-seq.

RNA EMSA

EMSA was performed using the LightShift Chemiluminescent RNA EMSA Kit (Thermo Fisher Scientific) as per instructions. Primary hippocampal neuron lysate was prepared as described in the pulldown assay. Protein (5 μg) was incubated with 100 ng of RNA (3′ end–labeled biotinylated probes were synthesized from Integrated DNA Technologies. The IRE control was used from the kit. Binding reactions were then run on a 6% polyacrylamide tris-boric acid–EDTA buffer (TBE) gel in 0.5× TBE buffer and transferred onto a nylon membrane for streptavidin–horseradish peroxidase–based detection of bands.

Silver staining and proteomics

Proteins were separated by SDS–polyacrylamide gel electrophoresis (PAGE), washed in water, and fixed overnight (10% glacial acetic acid and 30% ethanol) on an end-to-end shaker. Total protein bands were visualized using the Pierce Silver Staining Kit (Thermo Fisher Scientific). For MS, a large-scale pulldown from three combined experiments was run on SDS-PAGE, lanes corresponding to antisense and sense probe groups were cut out and processed for LC/MS-MS. Unique peptides were ascertained using Scaffold software.

Western blotting

Protein was isolated from whole cells, cell fractions, or RNA pulldown assays as described above and ultimately prepared in Laemmli buffer with 10% B-mercaptoethanol and 1% SDS. Equal volumes of protein were loaded for SDS-PAGE followed by overnight transfer to methanol-activated polyvinylidene difluoride membranes. Membranes were probed for PSD-95 (Thermo Fisher Scientific, MA1-045), GFP (Abcam, ab13970), actin (Abcam, Ab8227), synaptophysin (Abcam, ab32594), ankyrin B (Santa Cruz Biotechnology, sc-12718), spectrin-1 (Santa Cruz Biotechnology, sc-53444), and GAPDH (1:2000, Santa Cruz Biotechnology, sc-32233). The target proteins were detected using anti-rabbit or anti-mouse secondary antibodies (Cell Signaling Technology) at 1:5000 dilution and then visualized by Pierce ECL Western Blotting Substrate (Thermo Fisher Scientific). Blots were quantified using Fiji ImageJ.

Lentivirus preparation

PLL3.7 shRNA plasmid with lentivirus backbone was provided by the Xu laboratory. ADEPTR shRNA (mature sequence: 5′-GCTAGGTGCAAGATGGAA-3′) was then cloned into this backbone, replacing the scrambled sequence, and verified by Sanger sequencing (GENEWIZ). Each plasmid was cotransfected with helper plasmids (pMDL, pRev, and pVSVg) into human embryonic kidney (HEK) 293T cells using Mirus reagent. The medium was collected 48 to 72 hours later. Viral particles were concentrated and ultracentrifuged (25,000 rpm, 2.5 hours, 4°C) with sucrose gradient. The viral pellet was then resuspended in sterile PBS and stored at −80°C. Viral titer was determined by measuring GFP fluorescence after infection of HEK 293T cells with serial dilutions of the virus.

Statistical analysis

Statistical analysis was performed in R and Prism 8. Data are represented by the mean, and error bars represent SEM. Statistical tests performed are unpaired two-tailed *t* test, one-way and two-way ANOVA with Tukey's post hoc test, Dunnett's test, Holm's correction post hoc test, or pairwise *t* test, as indicated. *N* represents the number of independent wells of neurons for each experiment, unless stated otherwise.

SUPPLEMENTARY MATERIALS

Supplementary material for this article is available at http://advances.sciencemag.org/cgi/content/full/7/16/eabf0605/DC1

View/request a protocol for this paper from *Bio-protocol*.

REFERENCES AND NOTES

1. J. F. Guzowski, G. L. Lyford, G. D. Stevenson, F. P. Houston, J. L. McGaugh, P. F. Worley, C. A. Barnes, Inhibition of activity-dependent arc protein expression in the rat hippocampus impairs the maintenance of long-term potentiation and the consolidation of long-term memory. *J. Neurosci.* **20**, 3993–4001 (2000).
2. P. W. Frankland, C. O'Brien, M. Ohno, A. Kirkwood, A. J. Silva, α-CaMKII-dependent plasticity in the cortex is required for permanent memory. *Nature* **411**, 309–313 (2001).
3. S. Kaja, N. Sumien, P. K. Borden, N. Khullar, M. Iqbal, J. L. Collins, M. J. Forster, P. Koulen, Homer-1a immediate early gene expression correlates with better cognitive performance in aging. *Age* **35**, 1799–1808 (2013).
4. J. J. An, K. Gharami, G.-Y. Liao, N. H. Woo, A. G. Lau, F. Vanevski, E. R. Torre, K. R. Jones, Y. Feng, B. Lu, B. Xu, Distinct role of long 3' UTR BDNF mRNA in spine morphology and synaptic plasticity in hippocampal neurons. *Cell* **134**, 175–187 (2008).
5. C. R. Bramham, D. G. Wells, Dendritic mRNA: Transport, translation and function. *Nat. Rev. Neurosci.* **8**, 776–789 (2007).
6. S. Kim, K. C. Martin, Neuron-wide RNA transport combines with netrin-mediated local translation to spatially regulate the synaptic proteome. *eLife* **4**, e04158 (2015).
7. Y. Nakahata, R. Yasuda, Plasticity of spine structure: Local signaling, translation and cytoskeletal reorganization. *Front. Synaptic Neurosci.* **10**, 29 (2018).
8. M. Guttman, I. Amit, M. Garber, C. French, M. F. Lin, D. Feldser, M. Huarte, O. Zuk, B. W. Carey, J. P. Cassady, M. N. Cabili, R. Jaenisch, T. S. Mikkelsen, T. Jacks, N. Hacohen, B. E. Bernstein, M. Kellis, A. Regev, J. L. Rinn, E. S. Lander, Chromatin signature reveals over a thousand highly conserved large non-coding RNAs in mammals. *Nature* **458**, 223–227 (2009).
9. M. Guttman, P. Russell, N. T. Ingolia, J. S. Weissman, E. S. Lander, Ribosome profiling provides evidence that large noncoding RNAs do not encode proteins. *Cell* **154**, 240–251 (2013).
10. D. Li, J. Zhang, M. Wang, X. Li, H. Gong, H. Tang, L. Chen, L. Wan, Q. Liu, Activity dependent LoNA regulates translation by coordinating rRNA transcription and methylation. *Nat. Commun.* **9**, 1726 (2018).
11. B. L. Raveendra, S. Swarnkar, Y. Avchalumov, X.-A. Liu, E. Grinman, K. Badal, A. Reich, B. D. Pascal, S. V. Puthanveettil, Long noncoding RNA GM12371 acts as a transcriptional regulator of synapse function. *Proc. Natl. Acad. Sci. U.S.A.* **115**, E10197–E10205 (2018).
12. J. Valluy, S. Bicker, A. Aksoy-Aksel, M. Lackinger, S. Sumer, R. Fiore, T. Wüst, D. Seffer, F. Metge, C. Dieterich, M. Wöhr, R. Schwarting, G. Schratt, A coding-independent function of an alternative Ube3a transcript during neuronal development. *Nat. Neurosci.* **18**, 666–673 (2015).
13. S. Y. Grooms, K.-M. Noh, R. Regis, G. J. Bassell, M. K. Bryan, R. C. Carroll, R. S. Zukin, Activity bidirectionally regulates AMPA receptor mRNA abundance in dendrites of hippocampal neurons. *J. Neurosci.* **26**, 8339–8351 (2006).
14. S. J. Van Driesche, K. C. Martin, New frontiers in RNA transport and local translation in neurons. *Dev. Neurobiol.* **78**, 331–339 (2018).
15. L. Lipovich, F. Dachet, J. Cai, S. Bagla, K. Balan, H. Jia, J. A. Loeb, Activity-dependent human brain coding/noncoding gene regulatory networks. *Genetics* **192**, 1133–1148 (2012).
16. N. Mukherjee, L. Calviello, A. Hirsekorn, S. de Pretis, M. Pelizzola, U. Ohler, Integrative classification of human coding and noncoding genes through RNA metabolism profiles. *Nat. Struct. Mol. Biol.* **24**, 86–96 (2017).
17. D. Gobert, L. Topolnik, M. Azzi, L. Huang, F. Badeaux, L. DesGroseillers, W. S. Sossin, J.-C. Lacaille, Forskolin induction of late-LTP and up-regulation of 5' TOP mRNAs translation via mTOR, ERK, and PI3K in hippocampal pyramidal cells. *J. Neurochem.* **106**, 1160–1174 (2008).
18. E. Molnár, Long-term potentiation in cultured hippocampal neurons. *Semin. Cell Dev. Biol.* **22**, 506–513 (2011).
19. J. N. Gelinas, J. L. Banko, M. M. Peters, E. Klann, E. J. Weeber, P. V. Nguyen, Activation of exchange protein activated by cyclic-AMP enhances long-lasting synaptic potentiation in the hippocampus. *Learn. Mem.* **15**, 403–411 (2008).
20. S. Das, H. C. Moon, R. H. Singer, H. Y. Park, A transgenic mouse for imaging activity-dependent dynamics of endogenous Arc mRNA in live neurons. *Sci. Adv.* **4**, eaar3448 (2018).
21. M. F. Lin, I. Jungreis, M. Kellis, PhyloCSF: A comparative genomics method to distinguish protein coding and non-coding regions. *Bioinformatics* **27**, i275–i282 (2011).
22. L. Wang, H. J. Park, S. Dasari, S. Wang, J.-P. Kocher, W. Li, CPAT: Coding-Potential Assessment Tool using an alignment-free logistic regression model. *Nucleic Acids Res.* **41**, e74 (2013).
23. M. Terunuma, R. Revilla-Sanchez, I. M. Quadros, Q. Deng, T. Z. Deeb, M. Lumb, P. Sicinski, P. G. Haydon, M. N. Pangalos, S. J. Moss, Postsynaptic $GABA_B$ receptor activity regulates excitatory neuronal architecture and spatial memory. *J. Neurosci.* **34**, 804–816 (2014).
24. M. A. M. Franker, C. C. Hoogenraad, Microtubule-based transport - Basic mechanisms, traffic rules and role in neurological pathogenesis. *J. Cell Sci.* **126**, 2319–2329 (2013).
25. I. A. Muslimov, M. Titmus, E. Koenig, H. Tiedge, Transport of neuronal BC1 RNA in Mauthner axons. *J. Neurosci.* **22**, 4293–4301 (2002).
26. N. Otmakhov, L. Khibnik, N. Otmakhova, S. Carpenter, S. Riahi, B. Asrican, J. Lisman, Forskolin-induced LTP in the CA1 hippocampal region is NMDA receptor dependent. *J. Neurophysiol.* **91**, 1955–1962 (2004).
27. H. Murakoshi, H. Wang, R. Yasuda, Local, persistent activation of Rho GTPases during plasticity of single dendritic spines. *Nature* **472**, 100–104 (2011).
28. S. Swarnkar, Y. Avchalumov, B. L. Raveendra, E. Grinman, S. V. Puthanveettil, Kinesin family of proteins Kif11 and Kif21B act as inhibitory constraints of excitatory synaptic transmission through distinct mechanisms. *Sci. Rep.* **8**, 17419 (2018).
29. N. T. Ingolia, G. A. Brar, S. Rouskin, A. M. McGeachy, J. S. Weissman, The ribosome profiling strategy for monitoring translation *in vivo* by deep sequencing of ribosome-protected mRNA fragments. *Nat. Protoc.* **7**, 1534–1550 (2012).
30. C. Carrieri, L. Cimatti, M. Biagioli, A. Beugnet, S. Zucchelli, S. Fedele, E. Pesce, I. Ferrer, L. Collavin, C. Santoro, A. R. R. Forrest, P. Carninci, S. Biffo, E. Stupka, S. Gustincich, Long non-coding antisense RNA controls *Uchl1* translation through an embedded SINEB2 repeat. *Nature* **491**, 454–457 (2012).
31. S. V. Puthanveettil, RNA transport and long-term memory storage. *RNA Biol.* **10**, 1765–1770 (2013).
32. S. V. Puthanveettil, I. Antonov, S. Kalachikov, P. Rajasethupathy, Y. B. Choi, A. B. Kohn, M. Citarella, F. Yu, K. A. Karl, M. Kinet, I. Morozova, J. J. Russo, J. Ju, L. L. Moroz, E. R. Kandel, A strategy to capture and characterize the synaptic transcriptome. *Proc. Natl. Acad. Sci. U.S.A.* **110**, 7464–7469 (2013).
33. I. J. Cajigas, G. Tushev, T. J. Will, S. tom Dieck, N. Fuerst, E. M. Schuman, The local transcriptome in the synaptic neuropil revealed by deep sequencing and high-resolution imaging. *Neuron* **74**, 453–466 (2012).
34. A. Zappulo, D. van den Bruck, C. Ciolli Mattioli, V. Franke, K. Imami, E. McShane, M. Moreno-Estelles, L. Calviello, A. Filipchyk, E. Peguero-Sanchez, T. Müller, A. Woehler, C. Birchmeier, E. Merino, N. Rajewsky, U. Ohler, E. O. Mazzoni, M. Selbach, A. Akalin, M. Chekulaeva, RNA localization is a key determinant of neurite-enriched proteome. *Nat. Commun.* **8**, 583 (2017).
35. A. S. Hafner, P. G. Donlin-Asp, B. Leitch, E. Herzog, E. M. Schuman, Local protein synthesis is a ubiquitous feature of neuronal pre- and postsynaptic compartments. *Science* **364**, eaau3644 (2019).
36. T. J. Bell, K. Y. Miyashiro, J. Y. Sul, R. McCullough, P. T. Buckley, J. Jochems, D. F. Meaney, P. Haydon, C. Cantor, T. D. Parsons, J. Eberwine, Cytoplasmic BK_{Ca} channel intron-containing mRNAs contribute to the intrinsic excitability of hippocampal neurons. *Proc. Natl. Acad. Sci. U.S.A.* **105**, 1901–1906 (2008).
37. P. T. Buckley, M. T. Lee, J. Y. Sul, K. Y. Miyashiro, T. J. Bell, S. A. Fisher, J. Kim, J. Eberwine, Cytoplasmic intron sequence-retaining transcripts can be dendritically targeted via ID element retrotransposons. *Neuron* **69**, 877–884 (2011).
38. Y. H. Xing, R. W. Yao, Y. Zhang, C. J. Guo, S. Jiang, G. Xu, R. Dong, L. Yang, L. L. Chen, SLERT regulates DDX21 rings associated with Pol I transcription. *Cell* **169**, 664–678.e16 (2017).
39. Y. Zhang, X. O. Zhang, T. Chen, J. F. Xiang, Q. F. Yin, Y. H. Xing, S. Zhu, L. Yang, L. L. Chen, Circular intronic long noncoding RNAs. *Mol. Cell* **51**, 792–806 (2013).
40. D. Chakraborty, M. Paszkowski-Rogacz, N. Berger, L. Ding, J. Mircetic, J. Fu, V. Iesmantavicius, C. Choudhary, K. Anastassiadis, A. F. Stewart, F. Buchholz, lncRNA Panct1 maintains mouse embryonic stem cell identity by regulating TOBF1 recruitment to Oct-Sox sequences in early G1. *Cell Rep.* **21**, 3012–3021 (2017).
41. Q. F. Yin, L. Yang, Y. Zhang, J. F. Xiang, Y. W. Wu, G. G. Carmichael, L. L. Chen, Long noncoding RNAs with snoRNA ends. *Mol. Cell* **48**, 219–230 (2012).
42. D. Bernard, K. V. Prasanth, V. Tripathi, S. Colasse, T. Nakamura, Z. Xuan, M. Q. Zhang, F. Sedel, L. Jourdren, F. Coulpier, A. Triller, D. L. Spector, A. Bessis, A long nuclear-retained non-coding RNA regulates synaptogenesis by modulating gene expression. *EMBO J.* **29**, 3082–3093 (2010).
43. S. Keihani, V. Kluever, S. Mandad, V. Bansal, R. Rahman, E. Fritsch, L. Caldi Gomes, A. Gärtner, S. Kügler, H. Urlaub, J. D. Wren, S. Bonn, S. O. Rizzoli, E. F. Fornasiero, The long noncoding RNA *neuroLNC* regulates presynaptic activity by interacting with the neurodegeneration-associated protein TDP-43. *Sci. Adv.* **5**, eaay2670 (2019).
44. A. A. Butler, D. R. Johnston, S. Kaur, F. D. Lubin, Long noncoding RNA NEAT1 mediates neuronal histone methylation and age-related memory impairment. *Sci. Signal.* **12**, eaaw9277 (2019).
45. Y. Noda, R. Sato-Yoshitake, S. Kondo, M. Nangaku, N. Hirokawa, KIF2 is a new microtubule-based anterograde motor that transports membranous organelles distinct from those carried by kinesin heavy chain or KIF3A/B. *J. Cell Biol.* **129**, 157–167 (1995).
46. G. Morfini, S. Quiroga, A. Rosa, K. Kosik, A. Cáceres, Suppression of KIF2 in PC12 cells alters the distribution of a growth cone nonsynaptic membrane receptor and inhibits neurite extension. *J. Cell Biol.* **138**, 657–669 (1997).
47. T. Ogawa, N. Hirokawa, Microtubule destabilizer KIF2A undergoes distinct site-specific phosphorylation cascades that differentially affect neuronal morphogenesis. *Cell Rep.* **12**, 1774–1788 (2015).

48. N. Honkura, M. Matsuzaki, J. Noguchi, G. C. R. Ellis-Davies, H. Kasai, The subspine organization of actin fibers regulates the structure and plasticity of dendritic spines. *Neuron* **57**, 719–729 (2008).
49. M. W. Nestor, X. Cai, M. R. Stone, R. J. Bloch, S. M. Thompson, The actin binding domain of βI-spectrin regulates the morphological and functional dynamics of dendritic spines. *PLOS ONE* **6**, e16197 (2011).
50. G. Wang, D. J. Simon, Z. Wu, D. M. Belsky, E. Heller, M. K. O'Rourke, N. T. Hertz, H. Molina, G. Zhong, M. Tessier-Lavigne, X. Zhuang, Structural plasticity of actin-spectrin membrane skeleton and functional role of actin and spectrin in axon degeneration. *eLife* **8**, e38730 (2019).
51. C. Y.-M. Huang, C. Zhang, T. S.-Y. Ho, J. Oses-Prieto, A. L. Burlingame, J. Lalonde, J. L. Noebels, C. Leterrier, M. N. Rasband, αII spectrin forms a periodic cytoskeleton at the axon initial segment and is required for nervous system function. *J. Neurosci.* **37**, 11311–11322 (2017).
52. K. R. Smith, P. Penzes, Ankyrins: Roles in synaptic biology and pathology. *Mol. Cell. Neurosci.* **91**, 131–139 (2018).
53. N. Efimova, F. Korobova, M. C. Stankewich, A. H. Moberly, D. B. Stolz, J. Wang, A. Kashina, M. Ma, T. Svitkina, βIII spectrin is necessary for formation of the constricted neck of dendritic spines and regulation of synaptic activity in neurons. *J. Neurosci.* **37**, 6442–6459 (2017).
54. K. Nishimura, F. Yoshihara, T. Tojima, N. Ooashi, W. Yoon, K. Mikoshiba, V. Bennett, H. Kamiguchi, L1-dependent neuritogenesis involves ankyrinB that mediates L1-CAM coupling with retrograde actin flow. *J. Cell Biol.* **163**, 1077–1088 (2003).
55. C. F. Kline, J. Scott, J. Curran, T. J. Hund, P. J. Mohler, Ankyrin-B regulates $Ca_v2.1$ and $Ca_v2.2$ channel expression and targeting. *J. Biol. Chem.* **289**, 5285–5295 (2014).
56. P. Neumann, N. Jaé, A. Knau, S. F. Glaser, Y. Fouani, O. Rossbach, M. Krüger, D. John, A. Bindereif, P. Grote, R. A. Boon, S. Dimmeler, The lncRNA GATA6-AS epigenetically regulates endothelial gene expression via interaction with LOXL2. *Nat. Commun.* **9**, 237 (2018).
57. A. Bitetti, A. C. Mallory, E. Golini, C. Carrieri, H. Carreño Gutiérrez, E. Perlas, Y. A. Pérez-Rico, G. P. Tocchini-Valentini, A. J. Enright, W. H. J. Norton, S. Mandillo, D. O'Carroll, A. Shkumatava, MicroRNA degradation by a conserved target RNA regulates animal behavior. *Nat. Struct. Mol. Biol.* **25**, 244–251 (2018).
58. F. Niazi, S. Valadkhan, Computational analysis of functional long noncoding RNAs reveals lack of peptide-coding capacity and parallels with 3' UTRs. *RNA* **18**, 825–843 (2012).
59. S. Carpenter, D. Aiello, M. K. Atianand, E. P. Ricci, P. Gandhi, L. L. Hall, M. Byron, B. Monks, M. Henry-Bezy, J. B. Lawrence, L. A. J. O'Neill, M. J. Moore, D. R. Caffrey, K. A. Fitzgerald, A long noncoding RNA mediates both activation and repression of immune response genes. *Science* **341**, 789–792 (2013).
60. J. H. Yoon, K. Abdelmohsen, J. Kim, X. Yang, J. L. Martindale, K. Tominaga-Yamanaka, E. J. White, A. V. Orjalo, J. L. Rinn, S. G. Kreft, G. M. Wilson, M. Gorospe, Scaffold function of long non-coding RNA HOTAIR in protein ubiquitination. *Nat. Commun.* **4**, 2939 (2013).
61. H. Crerar, E. Scott-Solomon, C. Bodkin-Clarke, C. Andreassi, M. Hazbon, E. Logie, M. Cano-Jaimez, M. Gaspari, R. Kuruvilla, A. Riccio, Regulation of NGF signaling by an axonal untranslated mRNA. *Neuron* **102**, 553–563.e8 (2019).
62. B. D. Berkovits, C. Mayr, Alternative 3' UTRs act as scaffolds to regulate membrane protein localization. *Nature* **522**, 363–367 (2015).
63. R. Patro, G. Duggal, M. I. Love, R. A. Irizarry, C. Kingsford, Salmon provides fast and bias-aware quantification of transcript expression. *Nat. Methods* **14**, 417–419 (2017).
64. L. Stoppini, P. A. Buchs, D. Muller, A simple method for organotypic cultures of nervous tissue. *J. Neurosci. Methods* **37**, 173–182 (1991).
65. J. A. O'Brien, S. C. R. Lummis, Biolistic transfection of neuronal cultures using a hand-held gene gun. *Nat. Protoc.* **1**, 977–981 (2006).
66. L. A. Colgan, M. Hu, J. A. Misler, P. Parra-Bueno, C. M. Moran, M. Leitges, R. Yasuda, PKCα integrates spatiotemporally distinct Ca^{2+} and autocrine BDNF signaling to facilitate synaptic plasticity. *Nat. Neurosci.* **21**, 1027–1037 (2018).

Acknowledgments: We thank N. Kamasawa and L. Yan from the Max Planck Florida Institute for help with electron microscopy and fluorescence microscopy, respectively. We also acknowledge M. Kepiro for help with image analysis in ImageJ, P. Karunadharma at Scripps Florida Genomics Core for preparation of libraries for RNA-seq, and the Xu laboratory at Scripps Florida for providing the PLL3.7 shRNA plasmid. **Funding:** We acknowledge the funding support from NIH (5R01MH094607-05, 1R21DA039417-01A1, and 1R01MH119541-01A1 to S.V.P. and R01MH080047 and R35NS116804 to R.Y.) to carry out this work. **Author contributions:** E.G. designed and performed most experiments, analyzed the data, and wrote the manuscript. Y.N. performed all glutamate uncaging experiments in hippocampal slices and analyzed the data. Y.A. performed all electrophysiology experiments in primary hippocampal neuron cultures and analyzed the data. I.E. assisted with cell culture and pharmacology experiments and provided advice. S.S. supervised cell culture and imaging experiments and provided advice. R.Y. supervised the glutamate uncaging experiments and provided advice. S.V.P. supervised the project, designed experiments, and wrote the manuscript. **Competing interests:** The authors declare that they have no competing interests. **Data and materials availability:** All data needed to evaluate the conclusions in the paper are present in the paper and/or the Supplementary Materials. RNA-seq data related to fig. S1 were deposited to NCBI Gene Expression Omnibus with the accession number GSE157388, and all relevant data are available from the authors upon reasonable request.

Submitted 5 October 2020
Accepted 26 February 2021
Published 16 April 2021
10.1126/sciadv.abf0605

Citation: E. Grinman, Y. Nakahata, Y. Avchalumov, I. Espadas, S. Swarnkar, R. Yasuda, S. V. Puthanveettil, Activity-regulated synaptic targeting of lncRNA ADEPTR mediates structural plasticity by localizing Sptn1 and AnkB in dendrites. *Sci. Adv.* **7**, eabf0605 (2021).